AD_____

Award Number: W81XWH-09-1-0062

TITLE: Image Based Biomarker of Breast Cancer Risk: Analysis of Risk Disparity Among Minority Populations

PRINCIPAL INVESTIGATOR: Fengshan Liu

CONTRACTING ORGANIZATION: Delaware State University
Dover, DE 19901

REPORT DATE: March 2014

TYPE OF REPORT: Annual

PREPARED FOR: U.S. Army Medical Research and Materiel Command
Fort Detrick, Maryland 21702-5012

REPORT DOCUMENTATION PAGE

Form Approved
OMB No. 0704-0188

1. REPORT DATE *(DD-MM-YYYY)*	**2. REPORT TYPE**	**3. DATES COVERED** *(From - To)*
March 2014	Annual Report	1 Mar 2013 – 28 Feb 2014

4. TITLE AND SUBTITLE

Image Based Biomarker of Breast Cancer Risk:

Analysis of Risk Disparity Among Minority Populations

5a. CONTRACT NUMBER

5b. GRANT NUMBER
W81XWH-09-1-0062

5c. PROGRAM ELEMENT NUMBER

6. AUTHOR(S)
Fengshan Liu, Xiquan Shi, Charlie, Wilson, Dragoljub Pokrajac, Predrag Bakic, Andrew Maidment

email: fliu@desu.edu

5d. PROJECT NUMBER

5e. TASK NUMBER

5f. WORK UNIT NUMBER

7. PERFORMING ORGANIZATION NAME(S) AND ADDRESS(ES)

Delaware State University

Dover, DE 19901

8. PERFORMING ORGANIZATION REPORT NUMBER

9. SPONSORING / MONITORING AGENCY NAME(S) AND ADDRESS(ES)
U.S.Army Medical Research and Materiel Command
Fort Detrick, MD 21702-5012

10. SPONSOR/MONITOR'S ACRONYM(S)

11. SPONSOR/MONITOR'S REPORT NUMBER(S)

12. DISTRIBUTION / AVAILABILITY STATEMENT
Approved for public release; distribution unlimited.

13. SUPPLEMENTARY NOTES

14. ABSTRACT

During this no-cost extension year, we continued to do data analysis of the ACRIN database by improving original solutions with a construction of web-based data center for this project. By merging source data, converted data and computed data together to create a relational database and developing facilitating functions, we implemented various kinds of data selection requirements in terms of SQL statements, and apply further statistics routines to discover more hidden correlations among different quantifies. We updated the design of the software pipeline and a computer demo of real-time simulation of breast anatomy and imaging, and developed proof for computational complexity of the simulation algorithm and demonstrated its asymptotic efficiency.

15. SUBJECT TERMS
Breast Cancer, Risk Disparity, Minority Population, Image-Based Biomarker, Training Program

16. SECURITY CLASSIFICATION OF:			**17. LIMITATION OF ABSTRACT**	**18. NUMBER OF PAGES**	**19a. NAME OF RESPONSIBLE PERSON**
a. REPORT	**b. ABSTRACT**	**c. THIS PAGE**			USAMRMC
U	U	U	UU	54	**19b. TELEPHONE NUMBER** *(include area code)*

Standard Form 298 (Rev. 8-98)
Prescribed by ANSI Std. Z39.18

Table of Contents

Page

1. Introduction

During this no-cost extension year, we continued to do data analysis of the ACRIN database by improving original solutions with a construction of web-based data center for this project. By merging source data, converted data and computed data together to create a relational database and developing facilitating functions, we implemented various kinds of data selection requirements in terms of SQL statements, and apply further statistics routines to discover more hidden correlations among different quantifies. We updated the design of the software pipeline and a computer demo of real-time simulation of breast anatomy and imaging, and developed proof for computational complexity of the simulation algorithm and demonstrated its asymptotic efficiency.

2. Body

With this funded project, we will enhance DSU breast cancer research resources by: improving our expertise in translational and clinical breast cancer research; developing methods for computing image-based biomarkers for breast cancer risk, as well as methods for biomarker analysis of risk disparity; developing a database of clinical biomarkers computed from images of minority women; refining the existing and developing novel data mining techniques to determine the relationship between risk and image-based biomarkers. The improvement will support further growth of a sustained breast cancer research program at DSU and help establish us as a mid-Atlantic center for analysis of breast cancer risk and risk disparity among minority women.

The specific objectives of this training program include: (1) extending the skills of a select cadre of DSU faculty, so that they may become accomplished, influential and competitive breast cancer researchers; (2) establishing an independent breast cancer research program at DSU by performing a joint DSU–UPENN research project focused on breast cancer risk disparity in minority populations; and (3) producing a corpus of high quality published work and develop a portfolio of independently funded research grants at DSU to support a sustained breast cancer research program.

2.1 Objective 1

Extend the skills of a select cadre of Delaware State University (DSU) faculty, so that we may become accomplished, influential, and competitive breast cancer researchers.

- Organize specific training for selected DSU faculty, aimed at complementing our individual scientific background. (Y1-4); and

o Augment the faculty training by frequent communications with collaborating mentors and other renowned breast cancer researchers, by: (Y1-4)

2.1.1 Seminars and Conferences attended

- In August 2013, Dr. Bakic presented an invited talk on the Real Time Simulation of Breast Anatomy, at the 2013 AAPM Imaging Symposium on the Virtual Tools for the Validation of 3D/4D X-ray Breast Imaging, held in Indianapolis, IN. The related abstract was published in the July 2013 issue of Medical Physics. The presentation included our joint research results on improving the realism accelerating the breast anatomy simulation. The presentation also featured the activities of the AAPM Taskgroup TG234 on the Virtual Tools for Breast Imaging Validation. (Drs. Pokrajac and Bakic are members of TG234.)
- In December 2013, Dr. Maidment presented an Education Exhibit on the Role of Virtual Clinical Trials in Preclinical Testing of Breast Imaging Systems, at the 2013 RSNA Annual Meeting in Chicago, IL. At the same meeting, Dr. Bakic presented a scientific paper on the Automated and Optimized Software Platform for Virtual Clinical Trials. Both presentations were co-authored by Dr. Pokrajac, and featured results of our joint research on the breast imaging simulation.
- In February 2014, Drs. Pokrajac and Bakic attended the 2014 SPIE Medical Imaging conference in San Diego, CA to present a scientific paper on the Automated Simulation of Microcalcification Clusters in Software Breast Phantoms, as well as a Computer Demo of the Software Pipeline for Breast Imaging Simulation.
- Dr. Pokrajac presented results on partial volume simulation and mathematical issues of the simulation algorithm on XIII Serbia Mathematical Congress, 2014. Also he gave invited talk on Faculty of Electronics, Mechanical Engineering and Ship building and at Kolarac Institution in May 2014.

2.2 Objective 2

Establish an independent breast cancer research program at DSU by performing a joint DSU/Penn research project focused on breast cancer risk disparity in minority populations

o Obtain appropriate IRB approvals for the proposed research. (months 1-6 of Y1)

Included in Year 1 Report.

o Develop a database of anonymized clinical mammograms and patient metadata, obtained retrospectively

from ACRIN DMIST and Penn PPG trials. (Y1-Y2)

Included in Year 2 Report.

- Exploratory study (Drs. Wilson, Pokrajac, and Liu) Explore potential racial differences in genetic determinants of breast density. (Y2-Y4)

2.2.1. Analysis of Mammographic Images and Clinical Metadata of All Minority Women and the Age-Matched Caucasian Controls from the ACRIN DMIST Database

We continue to do the data analysis of the ACRIN database by improving original solutions with a construction of web-based data center for this project. By merging source data, converted data and computed data together to create a relational database and developing facilitating functions, we can easily implement various kinds of data selection requirements in terms of SQL statements, execute them to retrieve datasets to apply further statistics routines to discover more hidden correlations among different quantifies. Our findings include:

- The difference of the slope coefficients and determination coefficients for linear regression between big breasts that require two images for one breast and the normal or small breasts is relatively small, in the range of 10%, as shown in Fig 1. Therefore, we included the big breast images as samples for studies.
- The difference of the slope coefficients and determination coefficients for linear regression between MLO-positioned images and CC-positioned images is very large, over 100%, which confirms that the algorithm we employ to compute the density is better for the MLO-positioned images than the CC-positioned images, as shown by the comparison of Fig 2 and Fig 3. Therefore, we exclude the CC-positioned images as samples from now on until in the future we can find another way for computing density for CC-positioned images.
- Women's measured breast area does not correlate to the breast cancer risks, in other word, the regression coefficients are tiny, as shown in Fig 4.
- The data analysis confirms that the density is strongly, negatively correlated to women's age, which is a common sense for ordinary people, i.e, the younger women have denser breasts (Fig 5). Please note that the argument that younger women have denser breasts but lower immediately breast cancer is against the conjecture that denser breasts have higher breast cancer risk.
- The women's measured breast area is positively correlated to the women's age, i.e, the older women have the bigger breast area, as shown in Fig 6. This may be surprising on the first glimpse. However, the measured area is not the actual size, but the squeezed 2-D area of breasts. The finding above, i.e, younger women have denser breasts, and the fact that denser breasts have smaller room to be squeezed logically explain this finding.

- The data averaged by race does not support the conjecture that denser breasts have higher risk. Actually it is just other way around with large coefficient of determination, as show in Table 7. Of course, we realize that the Gail's model is subject to a large uncertainty for Hispanic/Latino.
- The finding 4 above suggests that the validity of the conjecture depends on the age. We find that in most age intervals, the breast density is positively but weakly correlated to the breast cancer risk, as shown in the Table 8. The linear regression coefficients indeed depend on the age heavily.
- In the age interval 40-45 and 62-72, the positive correlation between breast density and breast cancer risk is much stronger than other age intervals, as shown in Fig 9.

The findings above are based on our recent work of successful development of a web data center . The functions of the data center include (1) allowing user to design relational database on the web by providing a GUI interface to the web databases, (2) accepting data input from user manually or from remote application programs, (3) converting data from other data source format such as CSV file which is a common format for clinical data (4) allowing user to compose various queries to select data sets from various selection caritas, (5) displaying data as web pages and export data to Excel spreadsheets for performing further data analysis.

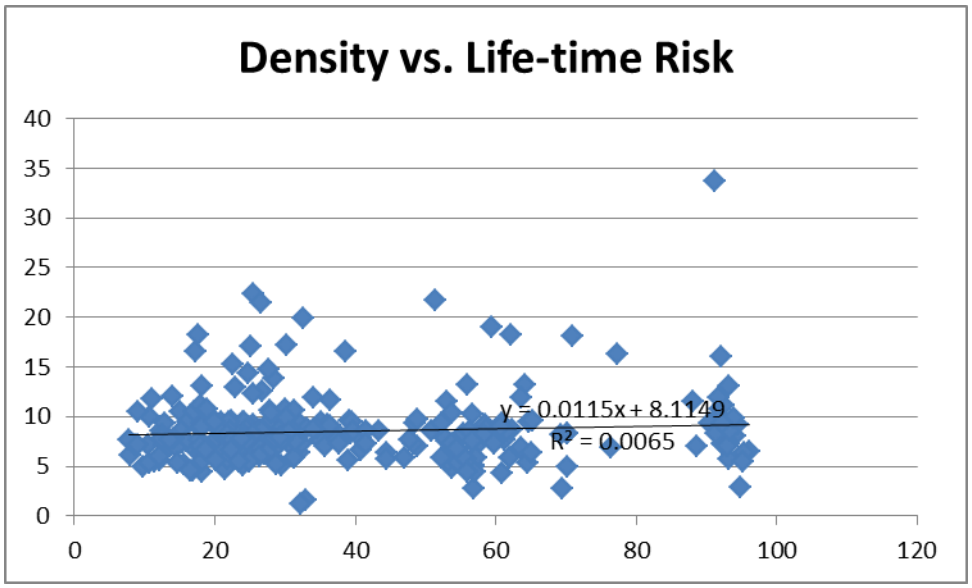

Fig 1. The linear regress plot of the breast density vs. life-time breast cancer risk for “big breast” women

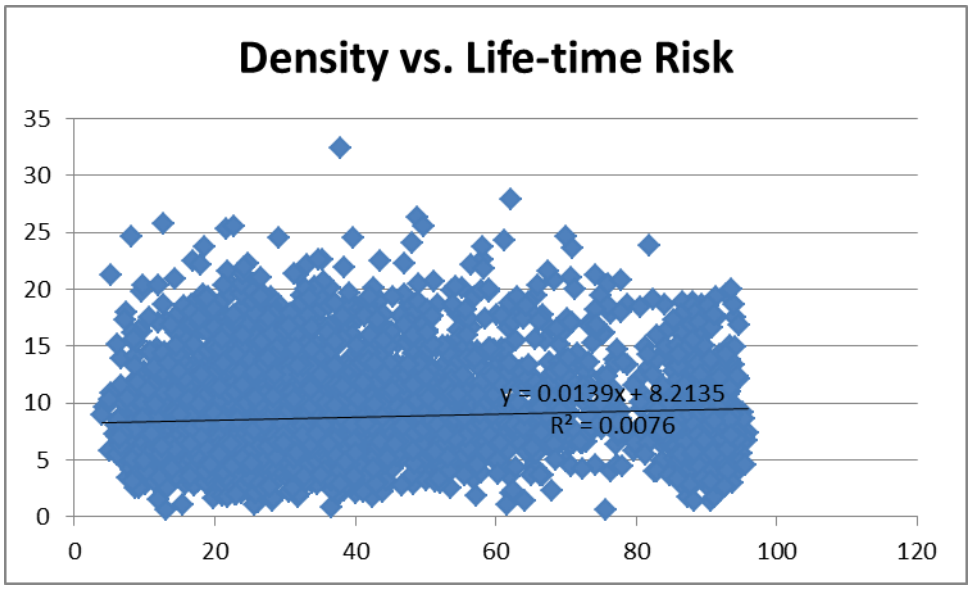

Fig 2. The linear regress plot of the breast density vs. life-time breast cancer risk for “normal-size” breast women (position: MLO)

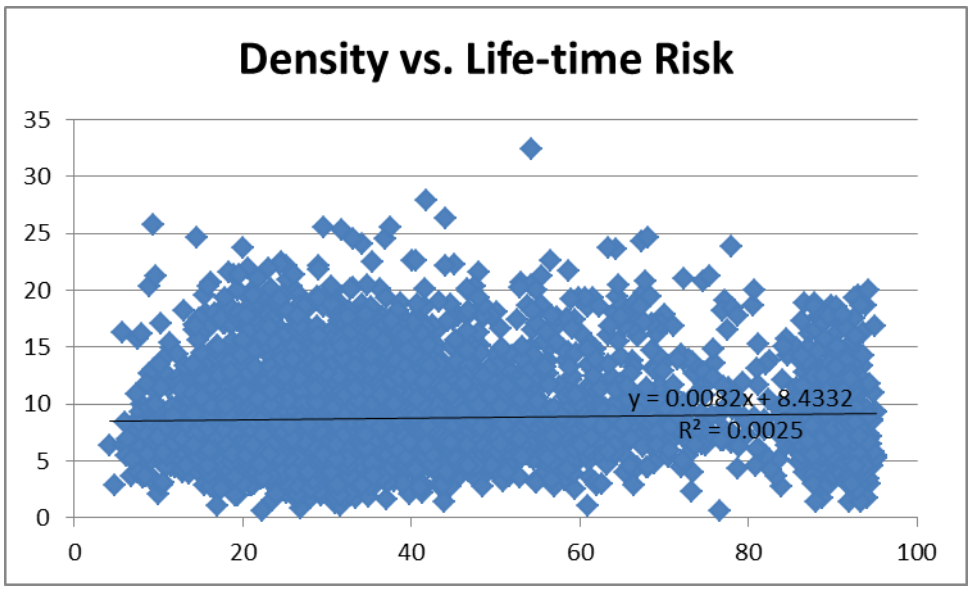

Fig 3. The linear regress plot of the breast density vs. Life-time breast cancer risk for “normal size breast” women (position: CC)

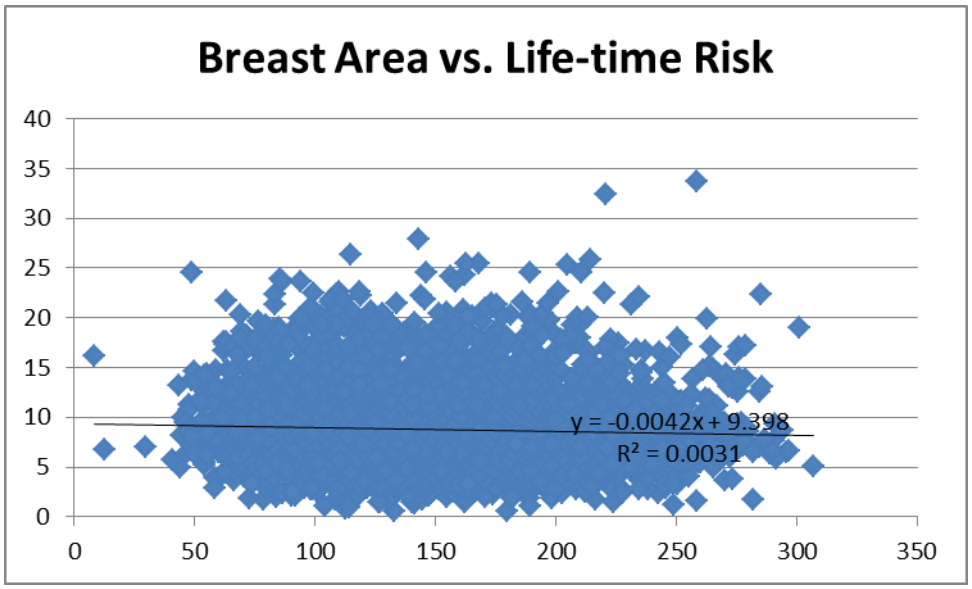

Fig 4. The weak correlation between breast area and life-time breast cancer risk

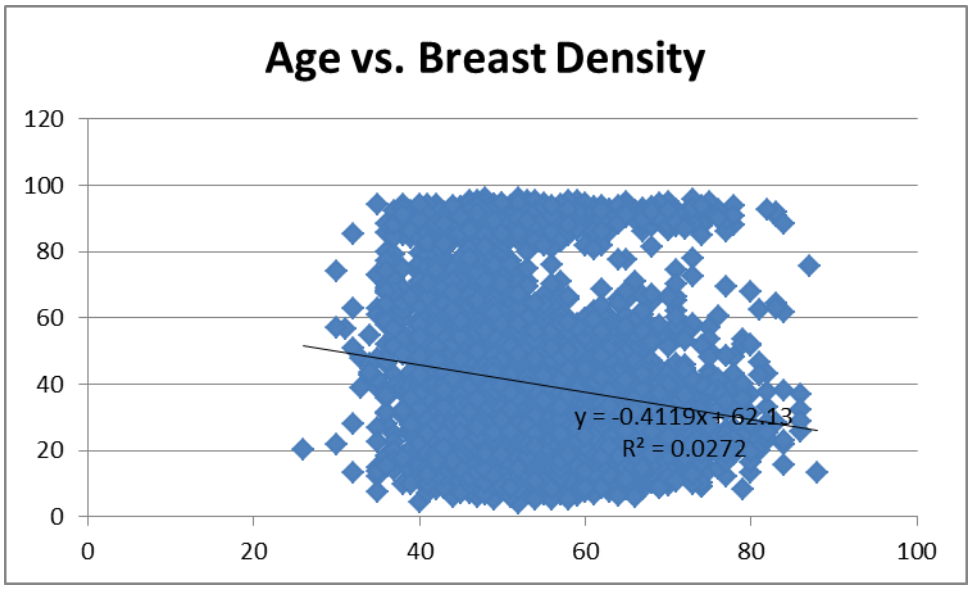

Fig 5. The strong negative correlation between Age and breast Density.

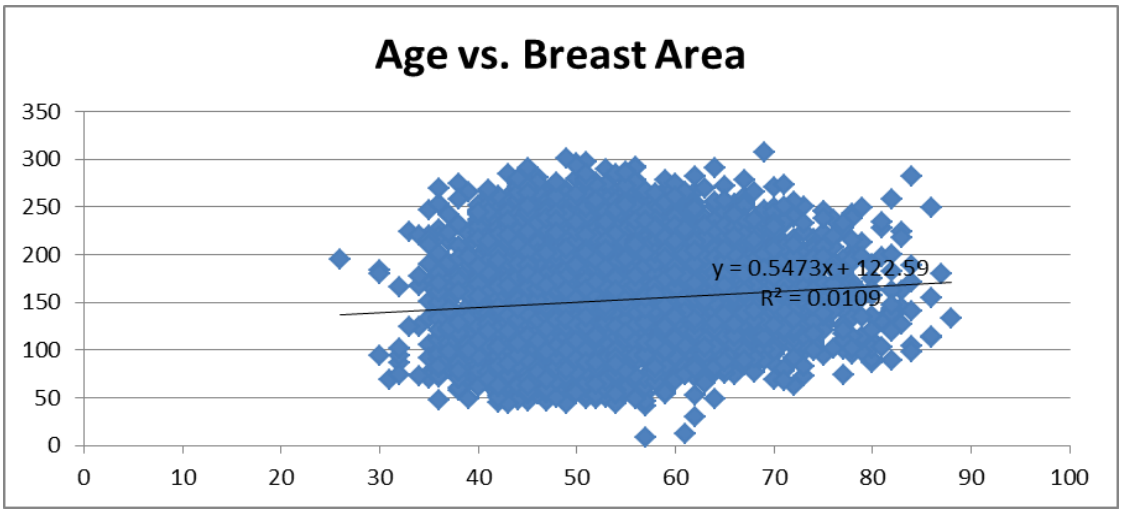

Fig 6. The strong positive correlation between women's age and the measured breast area

Race	Patients	Age	Images	Breast Area	Dense Area	Density	Risk 5Year	Risk Life
Asian	238	54.22	2.16	117.42	44.48	40.03	1.09	7.05
Black	1744	53.65	3.13	167.73	62.84	38.13	1.23	7.98
Hispanic /Latino	217	52.45	2.51	143.99	64.90	45.40	0.79	6.23
White	2481	53.74	2.56	144.89	56.97	40.88	1.38	9.69

Fig 7. The average numbers of interests by race

Center of Age Interval	Number of Patients	Slope of Linear Regression	Coefficients Of Determination
36	113	0.032843	0.023696
40	135	0.004559	7.67E-04
41	139	0.001818	1.41E-04
42	161	0.021103	0.014249
43	146	0.010153	0.003441
44	145	0.025072	0.023202
45	192	0.005164	0.001121
46	198	-0.0091	0.005601
47	182	-0.00683	0.001798
48	173	-0.01293	0.010095
49	176	5.00E-04	1.17E-05
50	175	0.00754	0.003063
51	210	-0.01771	0.012417
52	174	0.002875	3.99E-04
53	219	-0.00871	0.003447
54	176	-0.01311	0.007823
55	171	-5.32E-04	1.64E-05
56	158	0.016326	0.012772
57	158	-0.01571	0.01192
58	140	0.011876	0.006563
59	131	0.014717	0.011779
60	116	-0.0165	0.013812
61	118	-0.00179	2.53E-04
62	103	0.008103	0.003058
64	169	0.009127	0.006134
66	180	0.010356	0.011963
68	135	0.014086	0.018304
70	104	0.024838	0.097342
72	121	-0.00443	0.002877
76	109	-0.00644	0.010156
82	53	-0.00736	0.017216

Table 8. This table shows how and how much the breast density is correlated to the breast cancer risk in different age intervals. It shows that in most age interval, they are positively correlated.

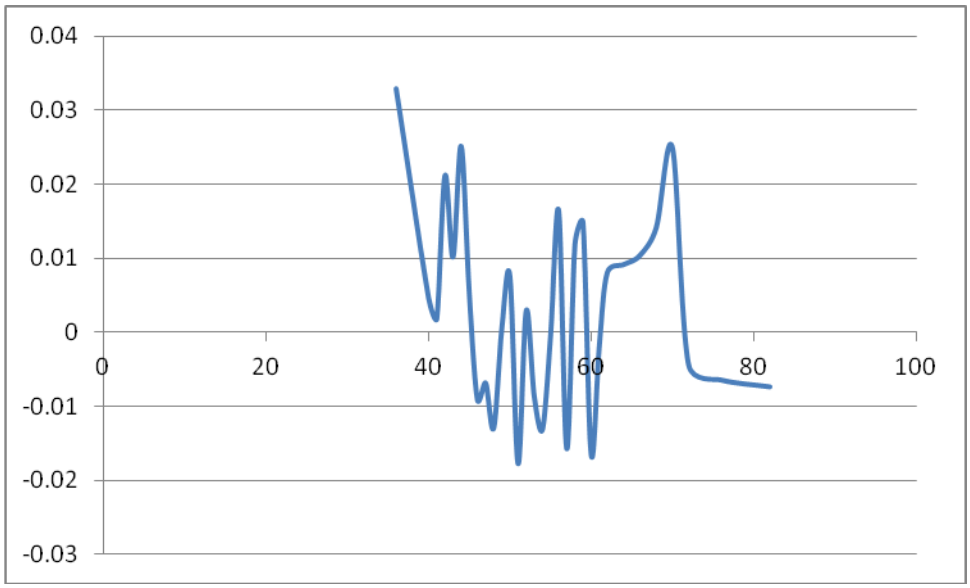

Fig 9. The distribution of the slope coefficient of linear regression over age. This picture shows that in the age interval of 40-45 and 62-72, the positive correlation between breast density and breast cancer risk is strong.

2.2.2. Mammogram Image Registration/Fusion

Image Registration by Using Spline Functions

Image registration is an image processing to transform different sets of data in which one has an overlap with another into one coordinate system. Usually, the data is multiple photographs such as the data from deferent sensors, times, depths, or viewpoints. Image registration is a very important and popular research field in image processing, not only because the requirement of the medical images processing such as Computational Anatomy(CA) which is applied to study health, disease and epidemiology and uses deformable mappings between images as a basic technique, but also because it is the basis for the application of the meteorological satellite spectral image data. There are various methods for image registration, such as affine, deformable DMFFD, diffeomorphic transformation method with MI, MSQ or CC as its similarity measure, thin spline method, landmark method and so on. Different from these methods, we introduced a new image registration method by using multivariate spline functions. The flexibility of constructing multivariate spline functions is one of the reasons that they are applied in image registration. That is, multivariate spline functions can be conveniently used to approximate real data locally. Actually, for the corresponding portions of an overlap part of two images, one can be locally treated as the image obtained by an affine transformation of the other. This indicates that we can partition two images into small parts and then register each small part onto its corresponding portion of the reference image. This is the basic idea of our spline image registration method. To facilitate the application with previous results, the range of multivariate spline function is taken as matrix variable. The basic idea of our method is as follow: we first translate one image, called reference image, into the output image, and

then register others, called source images, to the output image by spline functions. Since quadratic is the lowest possible degree to construct smooth multivariate splines, we first apply quadratic multivariate spline defined over Powell-Sabin type triangulations to image registration. The experiment results show that, comparing previous methods, the registration outputs have better matching and keep more details with better fair looking.

A novel breast image registration method is proposed to obtain a composite mammogram from several images with partial breast coverage, for the purpose of accurate breast density estimation. The breast percent density estimated as a fractional area occupied by fibroglandular tissue has been shown to be correlated with breast cancer risk. Some mammograms, however, do not cover the whole breast area, which makes the interpretation of breast density estimates ambiguous. One solution is to register and merge mammograms, yielding complete breast coverage. Due to elastic properties of breast tissue and differences in breast positioning and deformation during the acquisition of individual mammograms, the use of linear transformations does not seem appropriate for mammogram registration. Non-linear transformations are limited by the changes in the mammographic projections pixel intensity with different positions of the focal spot. We propose a novel method based upon non-linear local affine transformations. Our algorithm requires that feature points be extracted prior to registration, and the result of registration will depend on the reliability and accuracy of the extracted features. Automatic identification and extraction of feature points is difficult due to the non-linear compression deformation and the lack of significant landmarks in mammograms . We observe the prominent features (such as ducts and blood vessels) from both images. The crossing points are determined upon visual similarity in both mammograms. Due to compression and different positions of the breast, the coordinates of those crossing points may be different in the two mammograms, but the orientation of feature and local curvature of crossing points are more likely to be preserved. We also select other features (end points and middle points) in a small neighborhood around the selected crossing points. Subsequently, the deformation between two sets of feature points can be estimated. Given two sets of feature points in two images that need to be registered, we assume the deformation between them can be approximated by affine transformation, which can be considered as a first-order approximation of the true transformation resulting from breast projection. Finally, Shepherd interpolation is employed to compute affine transformations for the rest of the image area. The pixel values in the composite image are assigned using bilinear interpolation. We present preliminary results using the proposed approach applied to clinic mammograms taken from the ACRIN DMIST database of mammograms. This work is a part of a larger study of racial disparity in breast cancer risk. For that project, breast percent density and parenchymal texture of minority women and age-matched Caucasian controls from the ACRIN DMIST database are being compared. To date, we have been able to achieve anecdotal results that support continued development and testing of this new method. The proposed method is robust,

since the results of registration are similar regardless of the choice of the reference image. The observable features, especially the nipple and the boundary of skin, have good agreement. The results of the proposed method are comparable to the results of the diffeomorphic transform implemented using ANTs, an open source software package. Particularly, the textures of warped image are preserved in registered images, and the shape of registered image is similar as reference image. The registration error is smaller in the region of overlap (the upper part of the registered image), since we can extract the corresponding feature points only from this region. . The proposed transformation can be controlled locally. Moreover, the method is converging to the ground truth deformation if the paired feature points are evenly distributed and its number is large enough .In our future work, we plan to perform more extensive quantitative validation of the proposed algorithm on a series reference and warped images extracted from all the applicable images in the ACRIN DMIST database. Also, we will apply the technique to more images in the ACRIN DMIST database and develop statistical measures of the registration accuracy.

During this granting period Drs. Pokrajac and Bakic arranged several Skype teleconferences with the research lab of Dr. Aleksandar Peulic from the University of Kragujevac, Serbia, who continued the project previously performed by Dr. Feiyu Chen and Mr. Penglong Xu. Also, Dr. Pokrajac met Dr. Peulic nad his group at his research tip to Serbia in October 2013. Currently, Dr. Peulic is working on registration of mammographic images belonging to large breasts using ANTs software. The initial results indicate the possibility of good stitching of images belonging to the same breast.

2.2.3. Breast Phantom Simulation and Analysis

Software Pipeline for Breast Anatomy and Imaging Simulation

The pipeline connects anatomy and imaging simulation components, necessary for the performance of virtual clinical trials, for preclinical validation of breast imaging systems. The components are connected using the XML-based parsimonious data representation. Optimized simulation algorithms and their GPU-based implementation allows very fast (practically real time) simulation, supporting virtual trials with very large number of simulated anatomies. The pipeline design and simulation were discussed in our publications at 2013 AAPM, 2013 RSNA, and 2014 SPIE conferences.

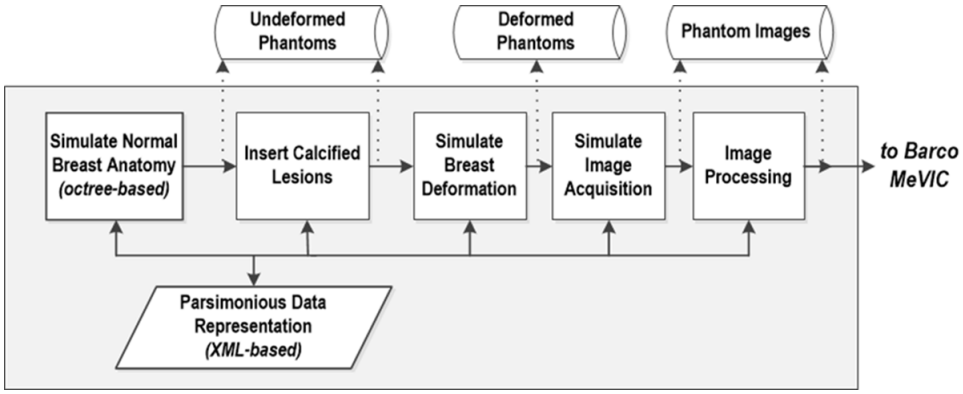

Fig 10. Flowchart of the Software Pipeline for Breast Anatomy and Imaging Simulation

Automated Insertion of Simulated Microcalcification Clusters into Software Breast Phantoms

3D clusters of microcalcifications, extracted from reconstructed clinical images, are inserted at randomly selected positions out of a set of the candidate positions. The candidate positions are identified based upon the assumptions about the origin of microcalcifications. Directed placement is based upon the assumption that clusters may occur only in non-adipose tissue regions; undirected placement presumes that clusters may be found anywhere inside the breast. In both cases, the candidate positions are identified by convolving a 3D rectangular hull (around the cluster) with phantom regions of non-adipose tissue (in case of directed placement) or with the breast interior (for undirected placement). These two placement strategies were validated in a 2-alternative forced choices observer study with 3 clinical radiologists as observers. Each observer reviewed 450 image pairs and indicated their preference between the directed and undirected placement. The study suggested observer's preference for undirected placement. More details are found in our 2014 SPIE talk.

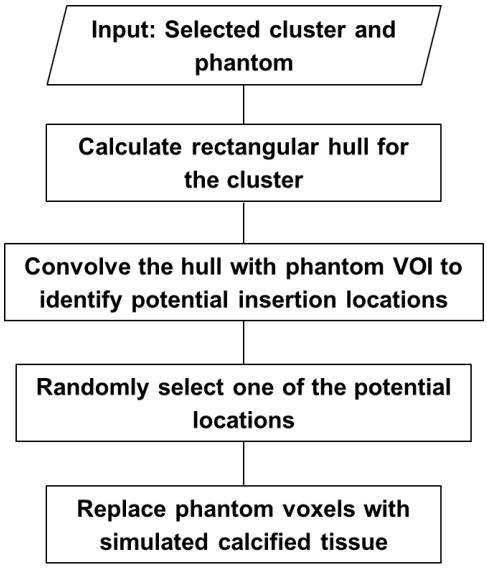

Fig 11. Flowchart of the method for automated insertion of simulated clusters into a software phantom

o Prepare peer-review publications on the results of the proposed research. (Y3-Y4)

Our manuscript about the simulation of partial volume is currently in review. Also, our manuscript on computational complexity of the recursive partitioning algorithm is in final stages of preparation and shall be submitted by August 2014. In addition, two papers were accepted for the 2014 International Workshop on Breast Imaging (IWDM), held in Gifu, Japan in July 2014. The papers describe our preliminary results on the simulation of small scale tissue structures by subdivision of phantom adipose compartments, as well as the preliminary results in the correlation between topological and textural properties extracted from clinical breast images. Both properties have been previously related with the breast cancer risk, thus their correlation may offers an improved estimation of risk.

o Validate success of the research training program by annual teleconferences with and bi-annual visits by external Advisory Committee.

N/A

1.3 Objective 3

Produce a corpus of high-quality published work and develop a portfolio of independently funded research grants at DSU to support a sustained breast cancer program

- See Reportable outcomes for publications
- Submitted a revised version of our NIH R01 grant proposal to the RFA on the Continued Development of Biomedical Software (**PAR-11-028):** http://grants.nih.gov/grants/guide/pa-files/PAR-11-028.html) D. Pokrajac, P. Bakic, A. Maidment
- Submitted a Delaware INBRE pilot proposal "Improving Realism of Software Breast Phantoms" (D. Pokrajac). The proposal has been funded in the amount of $160,000.

3. Important Findings

- Updated the design of the software pipeline for real-time simulation of breast anatomy and imaging.
- Developed a computer demo of the real-time simulation of breast anatomy and imaging
- Developed an automated method for the insertion of calcification clusters into software breast phantoms, and validated the method in observer trial with clinical radiologists as observers.
- Developed preliminary method for the simulation of small scale tissue structures
- Performed preliminary analysis of the correlation between topological and textural properties extracted from clinical breast images
- Developed preliminary algorithm for modeling of ducts

- Developed proof for computational complexity of the simulation algorithm and demonstrated its asymptotic efficiency
- Developed a web-based data center for this project, which includes database design and merge of source data, converted data and computed data together into relational database tables
- Developed facilitating functions allowing us to implement various data selection requirements in terms of SQL statements that can be executed to retrieve datasets for statistic software to take as input
- Confirmed that the validity of the conjecture that denser breasts have high breast cancer risk depends on age, i.e., in certain age intervals, the positive correlation does exists

4. Reportable Outcomes

Publications (journal papers and conference proceedings):

- Bakic, P., Myers, K., Reiser, I., Kiarashi, N., Zeng., R.: "Virtual Tools for Validation of X-ray Breast Imaging Systems," Medical Physics, 40: 3133. 2013.
- Bakic, P.R., Maidment, A.D.A., Chui, J.H., Avanaki, A.N., Marchessoux, C., Pokrajac, D.D, Espig, K., Kimpe, T., Xthona, A., Lago, M., Shankla, V.: "Automated and optimized imaging simulation platform for virtual clinical trials of breast cancer screening." In Proc. of the Scientific Assembly and Annual Meeting of the Radiological Society of North America, 2013.
- Maidment, A.D.A., Bakic, P.R., Chui, J.H., Avanaki, A.N., Marchessoux, C., Pokrajac, D.D, Espig, K., Kimpe, T., Xthona, A., Lago, M., Shankla, V.: "The role of virtual clinical trials in preclinical testing of breast imaging systems." In Proc. of the Scientific Assembly and Annual Meeting of the Radiological Society of North America, 2013.
- Shankla, V., Pokrajac, D.D., Weinstein, S.P., Conant, E.F., Maidment, A.D.A., Bakic, P.R.: "Automatic insertion of simulated microcalcification clusters in a software breast phantom," In Physics of Medical Imaging, Proc. SPIE 9033, ed. by B. Whiting, C. Hoeschen, D. Kontos, 2014.
- Abbey, C.K., Bakic, P.R., Pokrajac, D.D., Maidment, A.D.A., Eckstein, M.P., Boone, J.M.: "Non-Gaussian Statistical Properties of Virtual Breast Phantoms," In Image Perception, Observer Performance, and Technology Assessment, Proc. SPIE 9037, edited by C. Mello-Thoms, M. Kupinski, 2014.
- P. Bakic, D.Pokrajac, R.DeCaro, A.Maidment, "Realistic simulation of breast tissue microstructure in software anthropomorphic phantoms," *Proc. IWDM 2014,* in press.

- T. Nuzhnaya, A. Skoura, G. Cardenosa, V. Megalooikonomou, D. Kontos, D. Pokrajac, P. Bakic, A. Maidment, "Correlation between topological descriptors of the breast ductal network extracted from clinical galactograms and texture features of corresponding mammograms," *Proc. IWDM 2014,* in press.

Presentations:

- Breast Tissue Simulation with Recursive Partitioning Algorithm, Faculty of Electronics, Mechanical Engineering and Ship building, Split, Croatia, May 21, 2014 (Pokrajac, Bakic, Maidment), invited talk

- Simulation of Breast Tissues using Computer Algorithms, Kolarac Institution, Belgrade, Serbia, May 30. 2014 (Pokrajac, Bakic, Maidment), invited talk

- Partial volume simulation in software breast phantoms, XIII Serbian Mathematical Congress, Vrnjacka Banja, Serbia, May 23, 2014 (Pokrajac, Bakic, Maidment, Shi, Chen)

- Mathematical Issues in Software Breast Phantom Simulation, XIII Serbian Mathematical Congress, Vrnjacka Banja, Serbia, May 23, 2014 (Pokrajac, Maidment, Petkovic, Bakic), invited talk

5. Conclusion

During the last no-cost extension year, we focused on joint research between DSU and UPENN. We have addressed several issues related to racial disparity in breast cancer. In particular, we observed correlation between demography variables and the estimated cancers risk. We tested several methods co-registering mammograms containing multiple images .We have considered linear correlation between textures of mammograms and the graph theoretic measures of ductal network. The initial results indicated significant correlation for particular texture features. We continued our simulation efforts in verifying the optimal placement calcifications in simulated 3D phantoms. Also, we worked on the entropy-based phantom validation techniques on our phantom. We provided the mathematic proof that sets the algorithmic complexity boundaries of the simulation algorithm and demonstrates its asymptotic optimality. Our work in progress include further research on the optimal co-registration, correlation of texture and galactograms and further development of simulation for subcutaneous tissue and milk ducts.

6. References

N/A

7. Appendices

- Shankla, V., Pokrajac, D.D., Weinstein, S.P., Conant, E.F., Maidment, A.D.A., Bakic, P.R.: "Automatic insertion of simulated microcalcification clusters in a software breast phantom," In Physics of Medical Imaging, Proc. SPIE 9033, ed. by B. Whiting, C. Hoeschen, D. Kontos, 2014.
- Abbey, C.K., Bakic, P.R., Pokrajac, D.D., Maidment, A.D.A., Eckstein, M.P., Boone, J.M.: "Non-Gaussian Statistical Properties of Virtual Breast Phantoms," In Image Perception, Observer Performance, and Technology Assessment, Proc. SPIE 9037, edited by C. Mello-Thoms, M. Kupinski, 2014.
- P. Bakic, D.Pokrajac, R.DeCaro, A.Maidment, "Realistic simulation of breast tissue microstructure in software anthropomorphic phantoms," *Proc. IWDM 2014*, in press.
- T. Nuzhnaya, A. Skoura, G. Cardenosa, V. Megalooikonomou, D. Kontos, D. Pokrajac, P. Bakic, A. Maidment, "Correlation between topological descriptors of the breast ductal network extracted from clinical galactograms and texture features of corresponding mammograms," *Proc. IWDM 2014*, in press.

Automatic insertion of simulated microcalcification clusters in a software breast phantom

Varsha Shankla*, David D. Pokrajac[a], Susan P. Weinstein, Michael DeLeo,
Catherine Tuite, Robyn Roth, Emily F. Conant, Andrew D.A. Maidment, Predrag R. Bakic
Department of Radiology, University of Pennsylvania, Philadelphia, PA
[a]Computer and Information Sciences Department, Delaware State University, Dover, DE

ABSTRACT

An automated method has been developed to insert realistic clusters of simulated microcalcifications (MCs) into computer models of breast anatomy. This algorithm has been developed as part of a virtual clinical trial (VCT) software pipeline, which includes the simulation of breast anatomy, mechanical compression, image acquisition, image processing, display and interpretation. An automated insertion method has value in VCTs involving large numbers of images. The insertion method was designed to support various insertion placement strategies, governed by probability distribution functions (pdf). The pdf can be predicated on histological or biological models of tumor growth, or estimated from the locations of actual calcification clusters. To validate the automated insertion method, a 2-AFC observer study was designed to compare two placement strategies, undirected and directed. The undirected strategy could place a MC cluster anywhere within the phantom volume. The directed strategy placed MC clusters within fibroglandular tissue on the assumption that calcifications originate from epithelial breast tissue. Three radiologists were asked to select between two simulated phantom images, one from each placement strategy. Furthermore, questions were posed to probe the rationale behind the observer's selection. The radiologists found the resulting cluster placement to be realistic in 92% of cases, validating the automated insertion method. There was a significant preference for the cluster to be positioned on a background of adipose or mixed adipose/fibroglandular tissues. Based upon these results, this automated lesion placement method will be included in our VCT simulation pipeline.

Keywords: Software breast phantom, simulated microcalcification clusters, volumetric distribution of breast microcalcifications, 2-AFC observer study

1. INTRODUCTION

A variety of new 3D breast imaging technologies (e.g., stereomammography, tomosynthesis and computed tomography) are currently undergoing clinical investigation. These modalities offer specific technical advantages, such as superior spatial or contrast resolution. However, before widespread clinical adoption can occur, any new breast imaging system must undergo optimization and pass clinical validation. To safely accelerate this process, we have developed a preclinical validation method in the form of virtual clinical trials (VCT), based upon computer simulations of breast anatomy, image acquisition and interpretation (1-4). Other simulations of breast imaging have also been reported (5-9). Breast anatomy simulation provides the flexibility needed to simulate a broad range of anatomical variations, while providing the ground truth of simulated tissues needed for quantitative validation.

The visibility of microcalcification (MCs) in clinical images is of critical importance for breast imaging, as MCs can be the only sign of early cancer. To conduct a VCT of early breast cancer screening comparing digital mammography (DM) and digital breast tomosynthesis (DBT), we developed a method to insert MC clusters into our existing breast anatomy model automatically. Simulation of MC clusters in breast images has been reported in the literature. MC clusters have been extracted from both biopsy specimen (10, 11) or mastectomy specimen (12) images. Here, we report on a method using clusters extracted from stereoscopic biopsy images (13, 14).

Previous reports used manually selected locations (11). Here, we implement two automated strategies for MC placement: "undirected" and "directed". Both strategies use an underlying probability distribution function (PDF) of potential cluster locations. In the undirected strategy, the PDF is uniform within the entire volume of the breast, while in

* VarshaSh@seas.upenn.edu, DPokrajac@desu.edu, [Susan.Weinstein | Michael.DeLeo | Catherine.Tuite | Robyn.Gartner | Emily.Conant | Andrew.Maidment | Predrag.Bakic]@uphs.upenn.edu

Medical Imaging 2014: Physics of Medical Imaging, edited by ruce R. hiting, Christoph oeschen, espina Kontos,
Proc. of SPIE Vol. 9033, 90331 · © 2014 SPIE · CCC code: 1605-7422/14/$18 · doi: 10.1117/12.2044337

the directed strategy, the PDF is based upon the breast anatomy. In this paper, we consider a directed strategy in which MC only occur within fibroglandular tissue regions. The insertion method and placement strategies were validated in a two-alternative forced-choice (2-AFC) observer study with three radiologist observers.

2. MATERIALS AND METHODS

2.1 Breast anatomy simulation

2.2.1 Simulation of normal breast tissue

The Penn anthropomorphic software phantom simulates the breast as a set of tissues arrayed spatially, including: skin, adipose tissue, fibroglandular tissue, and Cooper's ligaments. Compartments within a matrix of Cooper's ligaments are simulated using a recursive partitioning algorithm (4). The compartments are then filled with adipose or glandular tissue according to rules governing spatial distribution (15). The resulting compartments vary in shape and size, creating a realistic simulation of the breast parenchyma. Simulation parameters can be set to simulate the full breadth of breast anatomy observed clinically.

After the generation of the breast phantom, clinical mammographic compression of the phantom is modeled by deforming the uncompressed phantom using 3D finite element methods (16-18). Mammography and DBT image acquisition is currently simulated by ray tracing projections through the phantom, as described below. Processed DM and reconstructed DBT images are obtained using the Real-Time Tomography (RTT, Villanova, PA) image processing and reconstruction software (19).

2.1.2 Simulation of calcification clusters

MC clusters used in this work are from an existing database of 130 clusters segmented from anonymized stereoscopic breast biopsy images (13, 14). Each cluster in the database is stored as a 3D binary volume, with a voxel value of '1' representing calcified material and a value of '0' representing the background tissue. Before insertion, each cluster is resampled to match the phantom voxel size. Since the clusters are most typically down-sampled, a fractional volume per voxel is calculated to preserve the quality of the MCs. Fig. 1 illustrates a selection of simulated MC clusters; the images were created by 3D rendering tomographic images in an orientation identical to that used in the study. Fig. 2 provides additional details regarding the 130 clusters available in the database. A histogram of the volume of individual MCs in shown in Fig. 2A; a histogram of the cluster volume is shown in Fig. 2B; and, a histogram of the number of MCs in a cluster is shown in Fig. 2C. These data show that the MCs and clusters used in the study are representative of those seen clinically.

(a) (b) (c)

Figure 1: 3D renderings of simulated clusters corresponding to (a) a benign fibroadenoma; (b) malignant DCIS (micropapillary grade 1); and (c) benign fibrocystic change with focal sclerosing adenosis.

2.2 Cluster insertion method

A flowchart of the automatic insertion method is shown in Fig. 3. The process begins with the selection of a phantom and a cluster to be inserted. A volume of interest (VOI) within the breast is determined based upon the probability distribution function of potential cluster locations. The software then searches for potential locations within the VOI. First, the minimum rectangular hull of the cluster (a rectangular prism that envelopes the cluster) is calculated. Then, the rectangular hull is convolved with the VOI to generate a set of candidate locations. The convolution is performed sequentially along the three orthogonal axes for computational expediency. The software then randomly selects one of

the candidate locations as the point of insertion. If the convolution does not return any candidate insertion points, then that phantom cannot be used with that cluster.

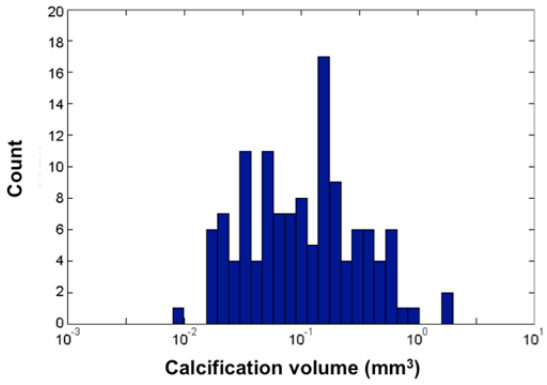

(a)

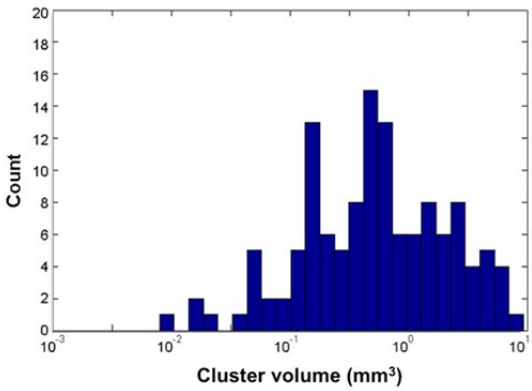

(b)

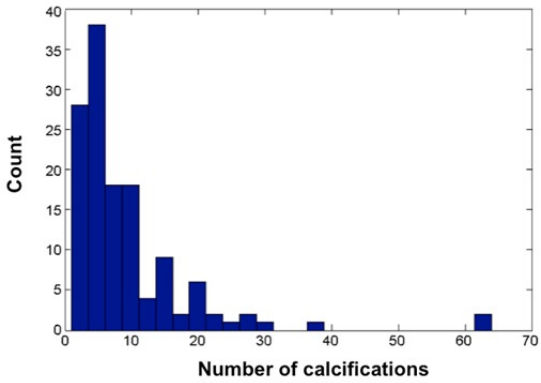

(c)

Figure 2: Histograms of (a) MC volume; (b) the cluster volume; (c) the number of MCs in a cluster.

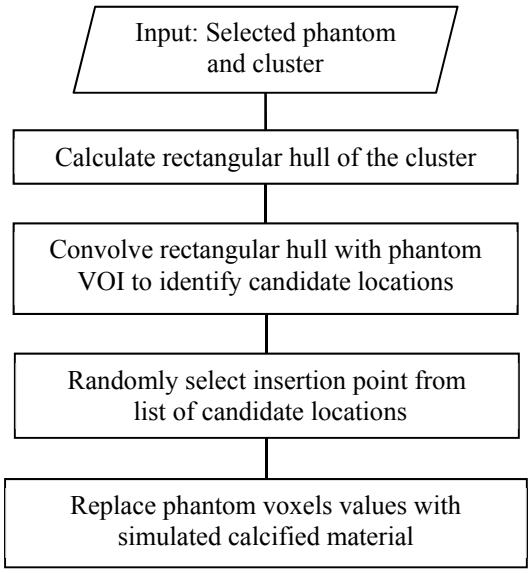

Figure 3: Flowchart of the automatic insertion process

A cluster is inserted into a phantom by replacing the voxel values of the phantom with calcified material (as detailed below) wherever the binary value of the cluster model is "1". In this work, the orientation of the cluster from the original database is preserved during insertion. Rotation of the cluster model would require recalculation of the rectangular hull. Rotation is one of the methods we intend to explore in the future to increase the variability of the cluster appearance.

We have evaluated both directed and undirected MC cluster placement strategies. The undirected strategy assumes that MCs can be located anywhere within the breast volume. The directed strategy assumes that the location of MCs is restricted in some sense. Here we implement a directed strategy based upon the assumption that MC clusters of clinical interest are not located within adipose tissue regions; that is, MCs originate from breast epithelial tissue. Thus, the VOI for the directed strategy consists of the set of all non-adipose phantom voxels. This VOI is convolved with the cluster rectangular hull to identify candidate insertion locations, as described above.

2.4 Simulation of mammographic projections

We simulated mammographic projections of the phantoms using a poly-energetic ray tracing method. Each voxel in the software phantom is associated with a linear attenuation coefficient, corresponding to the simulated tissue type. The voxels corresponding to inserted MCs were simulated as an admixture of calcified material and the background phantom tissue, with the linear attenuation coefficient given by:

$$\mu'(f,c) = f\mu_c c + (1-f)\mu_p \quad (1)$$

where μ' is the linear attenuation coefficient for a voxel in a phantom with a MC cluster; f is the fraction of the voxel volume occupied by the calcified tissue ($0<f<1$); μ_c is the linear attenuation coefficient of calcium hydroxyapatite; c is a parameter controlling the contrast of MCs in synthetic images ($0<c<1$); and μ_p is the linear attenuation coefficient of the phantom voxel before insertion. The resulting images were post-processed using a commercial image processing software package (Adara, Real Time Tomography, Villanova, PA) and saved in DICOM format.

2.5 Human observer study

We designed a 2-AFC observer study to validate the MC insertion method and compare the MC placement strategies. Images were created with both the directed and undirected placement strategies for every phantom-cluster pair from a set of phantoms and MC clusters. The observers were then required to select between images of the phantom produced with the two placement strategies.

Using a small pilot study (with one radiologist and 80 image pairs), we estimated that 450 image pairs were needed for the desired statistical power (Type II error < 0.05 with a Type I error of 0.05, resulting in an actual probability of a radiologist preferring direct placement in less than 42% of trials). To that end, we created 33 phantoms and selected 16 clusters from the database. The phantoms simulated a 450 ml breast with a thickness of 5 cm when compressed. Three sets of 11 phantoms each were created, with 15%, 20% and 30% volumetric glandularity, respectively. The clusters were selected based upon the number of individual MCs, and the spatial extent of the cluster. The number of MC in a cluster varied from 5 to 16. The cluster volume ranged from 0.008 to 9.328 mm^3. Among the 16 selected clusters, 10 were benign and six were malignant based on the pathology reports.

The image pairs for the 2-AFC study were generated by combining an image from each placement strategy for a given phantom-cluster pair. The left-right ordering of images, as well as the sequence of phantom-cluster pairs were randomized to avoid observer bias. Images were displayed using ViewDex (ver. 1.0_03; Sahlgrenska University Hospital and University of Gothenburg, Sweden) (20).

Each observer was instructed to select one image per pair based upon the plausibility of the cluster location in the phantom volume. For each image-pair shown, the observer was asked to answer four questions (see Fig. 4): (1) the visibility of the simulated cluster (in case of a negative answer, the remaining questions for the same image-pair were not considered for analysis); (2) the cluster realism (rated by five descriptive categories); (3) the preferred image of the pair; and (4) the confidence of the indicated preference (rated by a five category scale). The observer was instructed to select zero confidence if the observer had no preference between the images. The software recorded the answers along with elapsed time per image pair.

Three observers (all breast imaging fellows) participated in the 2-AFC study. During the study, we encouraged the observers to describe the rationale behind their preference, in terms of the MC cluster shape and location. The observer comments were recorded and matched with the appearance of simulated images.

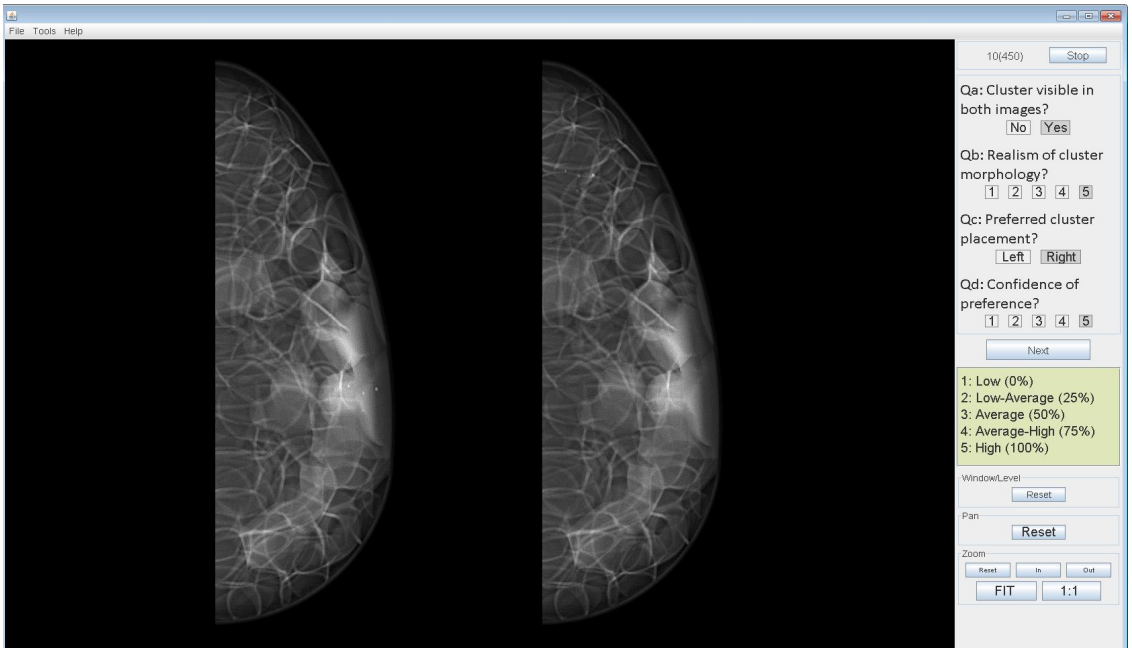

Figure 4: The 2-AFC observer study user interface, with an image pair and corresponding questions.

2.6 Statistical analysis

The observation data was analyzed as follows. Assume that a human observer is given a pair of images and with unknown probability p chooses a particular image. Let X=1 if the image with directed placement is chosen, and otherwise let X=0. The observer is provided a total of N image pairs. The random variable $Y = \sum_{i=1}^{N} X_i$ has a Binomial distribution with parameters N and p. Under the null-hypothesis, H_0, the observer does not have a preference between the directed and undirected strategies and p=0.5. To test H_0 vs. H_a (that the observer prefers undirected placement, p<0.5), we count the number of times, n, the observer chooses the directed placement. The p-value of the statistical test is computed as:

$$\text{p-value} = \sum_{i=0}^{n} \binom{N}{i} 0.5^i \, 0.5^{N-i} \tag{2}$$

We have also analyzed the dependence of the observers' preference on several factors, including the self-reported cluster realism level, the observer's confidence about the preference, the composition of the phantom at the location of cluster insertion, as well as the cluster location within the phantom.

3. RESULTS

3.1 Sections and projections of phantom with inserted MC clusters

Examples of the directed and undirected placement of MC clusters are shown in Figs. 5 and 6. Figure 5 shows the phantom and cluster in a single cross-section selected from the 3D volume. Figure 6 are projection images of the cluster after processing. These are typical of the images presented to the observers. We have added magnified regions of interest to aid in the review of the images for readers of this paper.

3.2 Observer study results

Overall preference of the directed cluster placement, calculated individually for each observer, as well as for all three observers combined, is shown in Table 1. The tabulated results indicate that the most of the clusters (93%) were visible. All the observers statistically significantly preferred the undirected placement strategy.

The observer's preference for insertion methods were further analyzed as a function of the confidence of their answers and cluster realism. The results are tabulated in Tables 2 and 3.

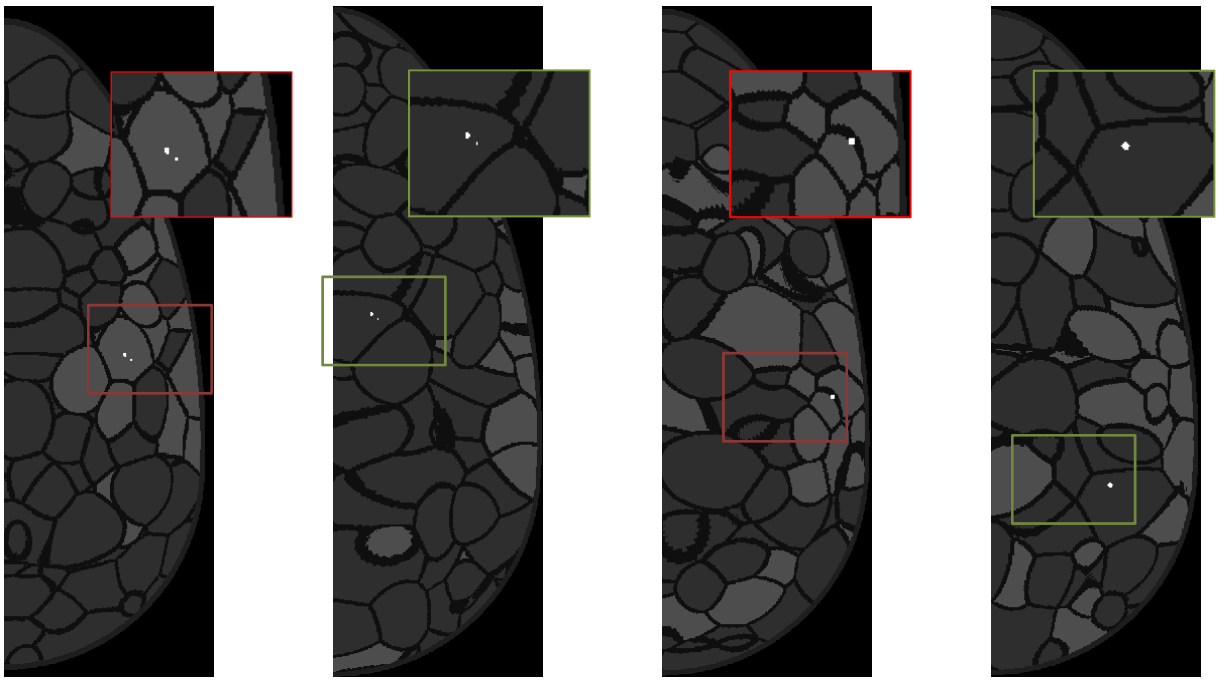

(a) (b) (c) (d)

Figure 5: Phantom slices illustrating two MC placement strategies. Enlarged are regions with inserted MCs. (a) A phantom with 15% glandularity, and directed placement; (b) the same phantom with undirected placement; (c) A phantom with 30% glandularity and directed placement; (d) the same phantom with undirected placement.

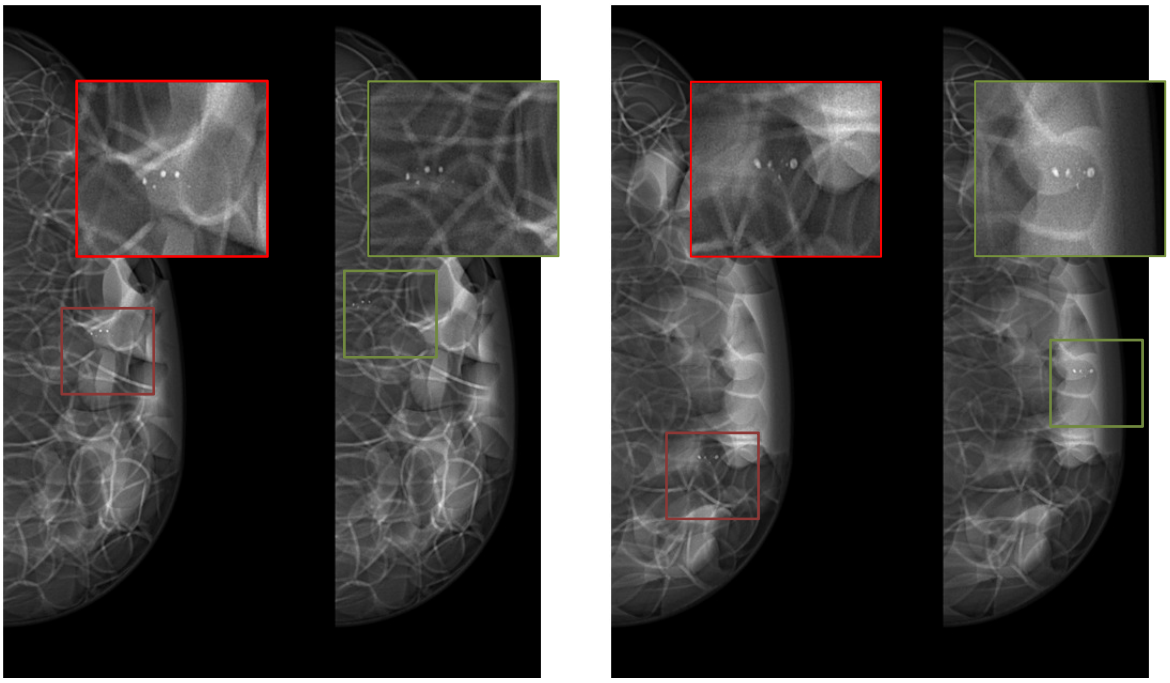

(a) (b)

Figure 6: Typical image pairs used in the validation study. Shown are synthetic mammographic projections corresponding to the phantoms from Fig. 5. Enlarged are regions with inserted MCs.

Table 1: Observer preference for the directed placement strategy.

Observer	Visible MCs (% of total)	Pref. directed (% of visible)	p-value
1	419 (93.11%)	169 (40.33%)	**4×10^{-5}**
2	416 (92.44%)	104 (25%)	**2×10^{-25}**
3	416 (92.44%)	136 (32.69%)	**7×10^{-13}**
All	1251 (92.67%)	409 (32.69%)	**3×10^{-25}**

Table 2: Observer preference for the directed strategy shown as a function of cluster realism.

Realism	Low (0%)	Low/Aver (25%)	Aver (50%)	Aver/High (75%)	High (100)
Observer 1					
Visible MCs (% total)	0 (0%)	62 (15%)	124 (30%)	278 (42%)	55 (13%)
Pref. directed (% visible)	0 (0%)	27 (44%)	62 (50%)	65 (37%)	15 (27%)
p-value	n/a	0.19	0.54	**2×10^{-4}**	**5×10^{-4}**
Observer 2					
Visible MCs (% total)	0 (0%)	33 (8%)	83 (20%)	155 (37%)	145 (35%)
Pref. directed (% visible)	0 (0%)	5 (8%)	25 (30%)	37 (24%)	37 (26%)
p-value	n/a	**3×10^{-5}**	**2×10^{-4}**	**2×10^{-11}**	**1×10^{-9}**
Observer 3					
Visible MCs (% total)	0 (0%)	2 (0.5%)	52 (12%)	356 (86%)	6 (1%)
Pref. directed (% visible)	0 (0%)	1 (50%)	19 (37%)	116 (33%)	0 (0%)
p-value	n/a	0.75	**0.04**	**2×10^{-11}**	n/a
All Observers					
Visible MCs (% total)	0 (0%)	97 (8%)	259 (21%)	689 (55%)	206 (16%)
Pref. directed (% visible)	0 (0%)	33 (34%)	106 (41%)	218 (32%)	52 (26%)
p-value	n/a	**1×10^{-3}**	**2×10^{-3}**	**1×10^{-22}**	**3×10^{-13}**

Table 3: Observer preference for the directed strategy shown as a function of decision confidence.

Confidence	Low (0%)	Low/Aver (25%)	Aver (50%)	Aver/High (75%)	High (100)
Observer 1					
Visible MCs (% total)	41 (10%)	64 (15%)	72 (17%)	209 (50%)	33 (8%)
Pref. directed (% visible)	16 (39%)	32 (50%)	34 (47%)	77 (37%)	10 (30%)
p-value	0.10	0.55	0.36	**9×10^{-5}**	**0.02**
Observer 2					
Visible MCs (% total)	19 (5%)	93 (22%)	71 (17%)	152 (37%)	81 (19%)
Pref. directed (% visible)	9 (47%)	34 (37%)	26 (37%)	29 (19%)	6 (7%)
p-value	0.50	**6×10^{-3}**	**0.02**	**3×10^{-15}**	**1×10^{-16}**
Observer 3					
Visible MCs (% total)	88 (21%)	180 (43%)	133 (32%)	14 (3%)	1 (0.2%)
Pref. directed (% visible)	44 (50%)	53 (29%)	34 (26%)	5 (36%)	0 (0%)
p-value	0.54	**2×10^{-8}**	**7×10^{-9}**	0.21	0.5
All Observers					
Visible MCs (% total)	148 (12%)	337 (27%)	276 (22%)	375 (30%)	115 (9%)
Pref. directed (% visible)	69 (47%)	119 (35%)	94 (34%)	111 (30%)	16 (14%)
p-value	0.23	**4×10^{-8}**	**6×10^{-8}**	**8×10^{-16}**	**4×10^{-16}**

As stated elsewhere in the paper, in the directed strategy, clusters were always positioned on a background of non-adipose tissues. In the undirected strategy, however, the cluster could be positioned over adipose and non-adipose tissues. Table 4 shows the observers' preference as a function of composition of background tissues, calculated as the percentage of non-adipose tissue in regions of phantoms that correspond to the rectangular hull of the inserted cluster.

Table 4: Observer preference as a function of the background composition of the undirected MC clusters.

Phantom % dense @ insertion location	**Very dense**	**Predom. dense**	**Average**	**Predom. fat**	**Very fatty**
Observer 1					
Visible MCs	49	5	20	66	58
Pref. directed (% vis.)	23 (47%)	2 (40%)	8 (40%)	25 (38%)	18 (31%)
p-value	4×10^{-1}	5×10^{-1}	2×10^{-1}	$\mathbf{3 \times 10^{-2}}$	$\mathbf{3 \times 10^{-3}}$
Observer 2					
Visible MCs	48	5	20	67	57
Pref. directed (% vis.)	21 (44%)	1 (20%)	8 (40%)	16 (24%)	11 (19%)
p-value	2×10^{-1}	2×10^{-1}	2×10^{-1}	$\mathbf{1 \times 10^{-5}}$	$\mathbf{2 \times 10^{-6}}$
Observer 3					
Visible MCs	47	5	20	66	59
Pref. directed (% vis.)	20 (43%)	2 (40%)	11 (55%)	24 (36%)	17 (29%)
p-value	2×10^{-1}	5×10^{-1}	8×10^{-1}	$\mathbf{2 \times 10^{-2}}$	$\mathbf{8 \times 10^{-4}}$
All Observers					
Visible MCs	144	15	60	199	174
Pref. directed (% vis.)	64 (44%)	5 (33%)	27 (45%)	65 (33%)	46 (26%)
p-value	1×10^{-1}	$\mathbf{2 \times 10^{-3}}$	$\mathbf{3 \times 10^{-3}}$	$\mathbf{6 \times 10^{-7}}$	$\mathbf{2 \times 10^{-10}}$

Based upon the known MC insertion locations, we plotted the distribution of preferred vs. non-preferred cluster locations, for the directed placement strategy (see Fig. 7).

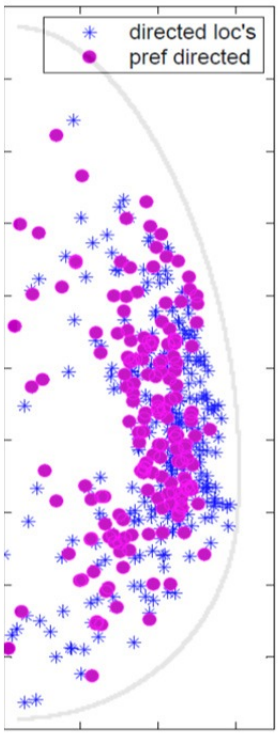

Figure 7: Graphical representation of the observer preference as a function of cluster location for one observer. The points mark the center location of each cluster placed according to the directed strategy for every image pair in study. The asterisk represent locations where the directed placement strategy placed MC clusters (but which were not preferred), and the circles represent locations were the directed points were preferred.

3.3 Observer comments

During the study, we recorded a number of insightful comments from observers about the appearance of simulated clusters and phantoms, and about the reasoning behind their preference for a specific image from an image pair. Several anecdotal comments are illustrated in Fig. 8.

"Very realistic, cluster with 2 punctuate and 1 indistinct calcification; pretty suspicious; less frequently seen this close to the nipple (referring to directed placement - left)"

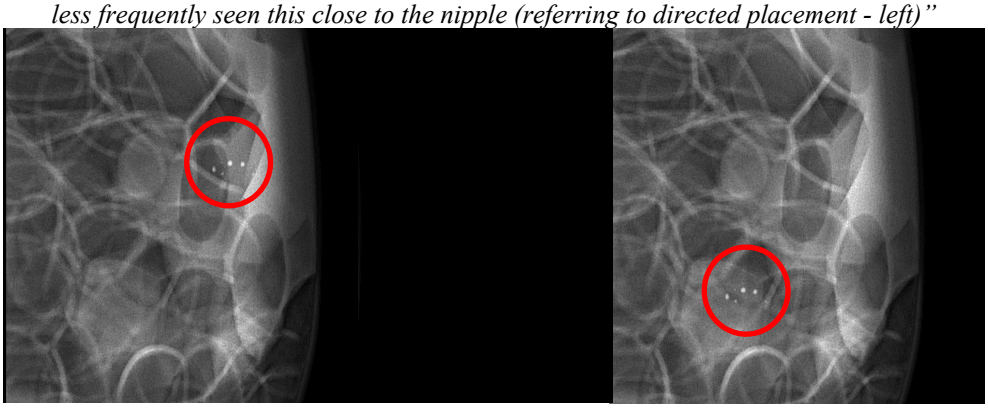

"The cluster looked too close to the skin; its appearance is similar to a fibroadenoma (with peripheral distribution on an oval shaped lesions). These lesions are rarely seen so close to the nipple; they are seen more frequently in the upper half (referring to directed placement - left)

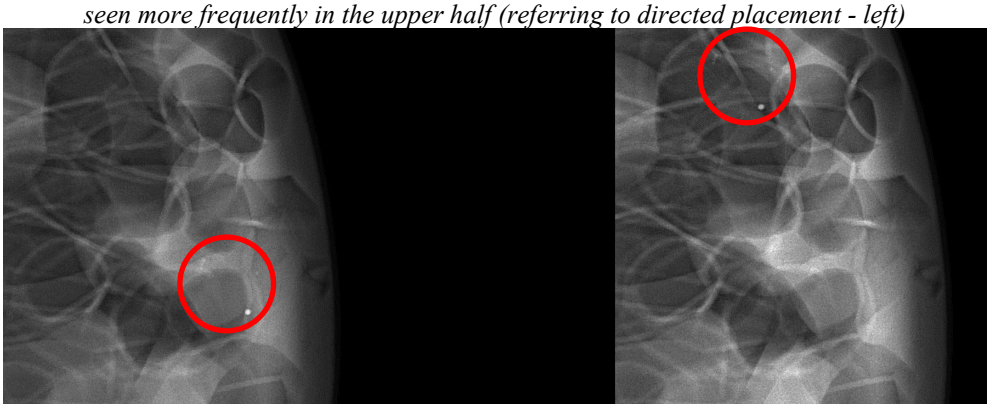

"Appearance of calcification with holes more typical for dermal regions and more plausible to be on posterior side (referring to undirected placement - right)"

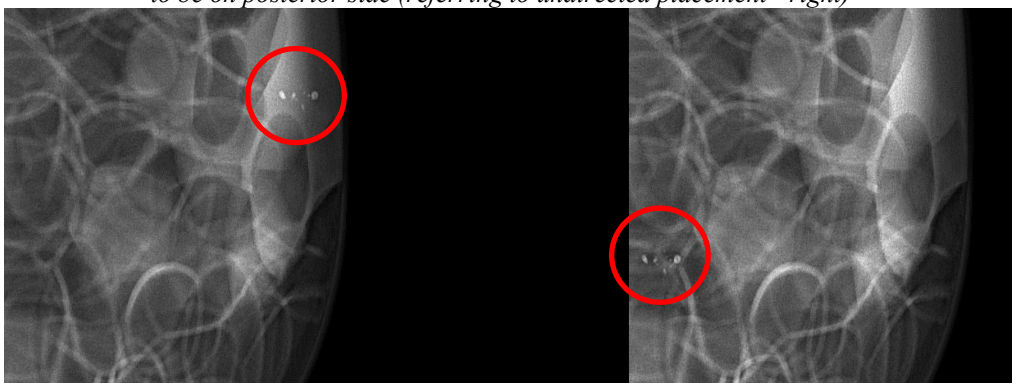

Figure 8: Synthetic image pairs in which radiologists commented upon the MC cluster. In these examples, the directed placement is on the left and the undirected placement is on the right. (Circles have been added to mark the cluster)

4. DISCUSSION

We have successfully implemented an automated method for insertion of simulated MC clusters into software breast phantoms, using two different placement strategies. A 2-AFC observer study with three radiologists has been used to validate the insertion method, and to identify the preferred placement strategy.

The analysis of cluster realism (Table 2) shows that the observers found that the simulated clusters have a high level of realism. In total, the observers found the cluster to be realistic (i.e., realism rated average or higher) in 92% of cases, validating the insertion method. This high level of realism supports our use of the automated insertion method. As such, it will now be fully incorporated and accelerated in our GPU-based VCT pipeline software.

The insertion method allows for the placement of MC clusters to be guided by a pdf. Two pdf were compared: a uniform pdf, and a pdf that placed MC clusters in fibroglandular tissue. The results of the preference study, summarized in Table 1, show that all observers statistically significantly preferred the undirected strategy. The directed strategy was preferred 33% of clusters, and undirected strategy was preferred in 67% of clusters. This indicates that the clusters did not look realistic on a background of glandular tissue.

Support for this premise is evident in Table 4, which shows the probability of selecting the directed strategy as a function of the background of the MC cluster in the image with undirected placement. These data do not show any preference for the placement strategy when the undirected placement strategy selected a MC cluster location within a dense tissue region. This result is sensible since the directed placement locations are, by definition, selected within dense tissue regions; thus, when both strategies select a dense background, the radiologists have no reason to prefer one strategy over the other.

Table 4 also shows that the preference for the placement of a cluster increases as the background composition at the insertion site becomes increasingly less dense. Thus, radiologists prefer clusters that are superimposed upon a predominantly adipose region. The observed preference may be due, in part, to the increased contrast of MCs in adipose regions. The adipose regions also have more visible simulated anatomical structures including prominent ligaments, potentially creating a set of features that aid in making diagnostic decisions about the detected cluster. As such, we plan to explore methods for adding structure in fibroglandular regions of our breast phantoms.

All the reported results from our observer study provide evidence that the undirected strategy produced more plausible simulations. It can be seen that as the observers' confidence increased (Table 3), the radiologists were more likely to prefer the undirected strategy. This evidence has led us to reject our original hypothesis about modeling MCs exclusively in dense phantom regions, which we justified by considering the epithelial origins of breast calcifications. Calcifications do originate from epithelial tissue histologically; however, it is now clear that we should not restrict potential MC cluster locations exclusively to dense mammographic regions.

An additional contributing factor may be that we currently simulate dense tissue regions as having a uniform composition within the interior of dense compartments. Thus, the glandular tissue may lack realism. We have previously tested other methods for simulating glandular tissue, including the use of subcompartments, (21) adding filtered binarized noise, (22, 23) or Perlin noise (24). As future work, we will test cluster realism with these various glandular tissue simulation methods.

Finally, Fig. 7 showed the preferred locations of MC clusters. It is clear that radiologists do not prefer MC clusters that are located near the distal edge of the breast. This finding is also supported by observers' comments, which not only prefer posterior locations, but also suggest that cluster location can lead to different interpretations of pathology. We plan to analyze observer preference as a function of cluster location, and intend to revise the placement strategy to improve realism further, if possible.

5. CONCLUSIONS

We have developed an automatic method to insert microcalcifications into software breast phantoms. This method was developed to help support VCTs that require large numbers of simulated breasts. We validated the insertion method in a 2-AFC study with radiologist observers. The radiologists found the resulting cluster placement to be realistic in 92% of cases. The insertion method allows for the placement of MC clusters to be guided by a probability density function. There was a significant preference for the cluster to be positioned on a background of adipose or mixed adipose/fibroglandular tissues. These results support our inclusion of this automated placement algorithm into our

simulation pipeline. Given that there was a strong preference for certain cluster locations, further research will be performed to continue to improve realism.

ACKNOWLEDGMENT

This work was supported in part by the US National Institutes of Health (R01 grant #CA154444), the US Department of Defense Breast Cancer Research Program (HBCU Partnership Training Award #BC083639), the US National Science Foundation (CREST grant #HRD-0630388 and III grant # 0916690), and the US Department of Defense/Department of Army (45395-MA-ISP, #54412-CI-ISP, W911NF-11-2-0046). The content is solely the responsibility of the authors and does not necessarily represent the official views of the NIH, NSF or DoD. The authors are thankful to Ms. Susan Ng from Real-Time Tomography (Villanova, PA) for processing the simulated projection images.

REFERENCES

1. Bakic PR, Albert M, Brzakovic D, Maidment ADA. Mammogram synthesis using a 3D simulation. II. Evaluation of synthetic mammogram texture. Medical Physics. 2002;29(9):2140-51.
2. Bakic PR, Albert M, Brzakovic D, Maidment ADA. Mammogram synthesis using a 3D simulation. I. Breast tissue model and image acquisition simulation. Medical Physics. 2002;29(9):2131-9.
3. Bakic PR, Zhang C, Maidment ADA. Development and Characterization of an Anthropomorphic Breast Software Phantom Based upon Region-Growing Algorithm. Medical Physics. 2011;38(6):3165-76.
4. Pokrajac DD, Maidment ADA, Bakic PR. Optimized generation of high resolution breast anthropomorphic software phantoms. Medical Physics. 2012;39(4):2290-302.
5. Bliznakova K, Suryanarayanan S, Karellas A, Paiilikarakis N. Evaluation of an improved algorithm for producing realistic 3D breast software phantoms: Application for mammography. Medical Physics. 2010;37(11):5604-17.
6. Li CM, Segars WP, Tourassi GD, Boone JM, Dobbins III JT. Methodology for generating a 3D computerized breast phantom from empirical data. Medical Physics. 2009;36(7):3122-31.
7. Chen B, Shorey J, Saunders RSJ, Richard S, Thompson J, Nolte LW, et al. An anthropomorphic breast model for breast imaging simulation and optimization. Academic Radiology. 2011;18(5):536-46.
8. O'Connor JM, Das M, Didier CS, Mahd M, Glick SJ. Generation of voxelized breast phantoms from surgical mastectomy specimens Medical Physics. 2013;40(4):041915.
9. Hoeschen C, Fill U, Zankl M, Panzer W, Regulla D, Dohring W. A high resolution voxel phantom of the breast for dose calculations in mammography. Radiation Protection Dosimetry 2005;114(1-3):406-9.
10. Shaheen E, Van Ongeval C, Cockmartin L, Zanca F, Marshall NW, Jacobs J, et al. Realistic Simulation of Microcalcifications in Breast Tomosynthesis. In: Marti Jea, editor. International Workshop on Digital Mammography (IWDM); Girona, Spain: Springer; 2010. p. 235-42.
11. Lefebvre F, Benali H, Gilles R, Di Paola R. A simulation model of clustered breast microcalcifications. Medical Physics. 1994;21(12):1865-74.
12. Warren LM, Green FH, Shrestha L, Mackenzie A, Dance DR, Young KC. Validation of simulation of calcifications for observer studies in digital mammography. Physics in Medicine and Biology. 2013;58:N217-N28.
13. Maidment ADA, Albert M, Conant EF. Three-dimensional imaging of breast calcifications. In: Selander JM, editor. 26th AIPR Workshop: Exploiting New Image Sources and Sensors; 1998; Washington, D.C.: SPIE; 1998. p. 200-8.
14. Maidment ADA, Albert M, Feig SA. 3-D Mammary Calcification Reconstruction from a Limited Number of Views. Physics of Medical Imaging; 1996; San Diego: SPIE; 1996. p. 378-89.
15. Chui JH, Zeng R, Pokrajac DD, Park S, Myers KJ, Maidment ADA, et al. Two methods for simulation of dense tissue distribution in software breast phantoms. Physics of Medical Imaging; lake Buena Vista, FL: SPIE; 2013.
16. Ruiter NV, Zhang C, Bakic PR, Carton A-K, Kuo J, Maidment ADA. Simulation of tomosynthesis images based on an anthropomorphic software breast tissue phantom. In: Miga MI, Cleary KR, editors. SPIE Medical Imaging: Visualization, Image-guided Procedures, and Modeling San Diego, CA2008.
17. Xia S, Liu F, Maidment ADA, Bakic PR. Refinements to the Deformation Model of an Anthropomorphic Computer Generated Breast Phantom. Medical Physics. 2010;37:3131.
18. Lago MA, Maidment ADA, Bakic PR. Modelling of mammographic compression of anthropomorphic software breast phantom using FEBio. Int'l Symposium on Computer Methods in Biomechanics and Biomedical Engineering; Salt Lake City, UT2013.
19. Kuo J, Ringer P, Fallows SG, Ng S, Bakic PR, Maidment ADA, editors. Dynamic reconstruction and rendering of 3D tomosynthesis images. Physics of Medical Imaging; 2011; Lake Buena Vista, FL: SPIE.

20. Hakansson M, Svensson S, Zachrisson S, Svalkvist A, Bath M, Mansson LG. ViewDEX: an efficient and easy-to-use software for observer performance studies. Radiation Protection Dosimetry. 2010;139:42-50.
21. Abbey CK, Bakic PR, Pokrajac DD, Maidment ADA, Eckstein MP, Boone JM. Non-Gaussian Statistical Properties of Virtual Breast Phantoms. In: Mello-Thoms CR, Kupinski MA, editors. SPIE Image Perception, Observer Performance, and Technology Assessment; San Diego, CA: SPIE; 2014.
22. Reiser I, Lau AB, Nishikawa RM, Bakic PR. A directional small-scale tissue model for an anthropomorphic breast phantom. International Workshop on Breast Imaging; Philadelphia, PA: Springer; 2012.
23. Lau AB, Reiser I, Nishikawa RM, Bakic PR. A statistically defined anthropomorphic software breast phantom Medical Physics. 2012;39(6):3375-85.
24. Timberg P. Technical optimisation of digital breast tomosynthesis for future breast screening. European Congres of Radiology; Vienna, Austria2014.

Non-Gaussian statistical properties of virtual breast phantoms

Craig K. Abbey*[ab], Predrag R. Bakic[c], David D. Pokrajac[d], Andrew D.A. Maidment[c], Miguel P. Eckstein[a], and John M. Boone[b]

[a]Dept. of Psychological and Brain Sciences, UC Santa Barbara, Santa Barbara, CA. USA 93106; [b]Dept of Radiology, UC Davis Medical Center, Sacramento CA. USA; [c]Department of Radiology, University of Pennsylvania, Philadelphia, PA. USA; [d]Department of Computer and Information Sciences, Delaware State University, Dover, Delaware. USA.

ABSTRACT

Images derived from a "phantom" are useful for characterizing the performance of imaging systems. In particular, the modulation transfer properties of imaging detectors are traditionally assessed by physical phantoms consisting of an edge. More recently researchers have come to realize that quantifying the effects of object variability can also be accomplished with phantoms in modalities such as breast imaging where anatomical structure may be the principal limitation in performance. This has driven development of virtual phantoms that can be used in simulation environments. In breast imaging, several such phantoms have been proposed. In this work, we analyze non-Gaussian statistical properties of virtual phantoms, and compare them to similar statistics from a database of breast images.

The virtual phantoms assessed consist of three classes. The first is known as clustered-blob lumpy backgrounds. The second class is "binarized" textures which typically apply some sort of threshold to a stochastic 3D texture intended to represent the distribution of adipose and glandular tissue in the breast. The third approach comes from efforts at the University of Pennsylvania to directly simulate the 3D anatomy of the breast. We use Laplacian fractional entropy (LFE) as a measure of the non-Gaussian statistical properties of each simulation.

Our results show that the simulation approaches differ considerably in LFE with very low scores for the clustered-blob lumpy background to very high values for the UPenn phantom. These results suggest that LFE may have value in developing and tuning virtual phantom simulation procedures.

Keywords: Laplacian Fractional Entropy, Breast phantoms, image statistics, and natural scene statistics

1. INTRODUCTION

The use of "virtual" breast phantoms for evaluating new breast imaging technology has many appealing qualities. These phantoms are the output of simulations of breast tissue, with the intent of capturing the effect of anatomical variability on the performance of imaging systems. As such, the "phantom" may be considered as the ensemble of image backgrounds produced by the simulation procedure. Virtual phantoms have advantages that arise from known ground truth about the object being imaged, and the ability to evaluate an unbuilt system through a subsequent simulation of the imaging process.

However, in order to be effective, a virtual phantom must accurately capture the effects of patient structured images. We will refer to this goal as phantom realism; a more realistic phantom will more fully capture anatomical effects than a less realistic phantom. But it is not clear at this point in time how to validate such a comparison, or how such a validation might depend on the task that drives development of the imaging system..

The approach we are exploring in this work is based on the idea that realism can be characterized by comparing statistical properties of the phantom ensemble (or the subsequent images) and actual patient images in cases where such images are available. Traditionally, statistical properties have been limited to the power-spectrum [1, 2], which characterize second-order statistical properties (i.e. variance, covariance, and correlations), under the assumption of stationarity. However, it is well known that the power spectrum does not fully capture the appearance

Medical Imaging 2014: Image Perception, Observer Performance, and Technology Assessment, edited by Claudia R. Mello-Thoms, Matthew A. Kupinski, Proc. of SPIE Vol. 9037, 90370G

of some medical images [3]. For example, it is generally easy to differentiate between a real patient mammogram and a Gaussian process that has matched the power spectrum of the mammograms. Figure 1 gives examples of each of these. The top row shows breast images from clinical exams that have been log-converted to density (note that we have not applied the usual "for-display" processing to these images since we are interested in the properties of the objects being imaged, and no necessarily the final displayed image). We contend that various textural components of the mammograms make them readily discriminable for the matched Gaussian textures.

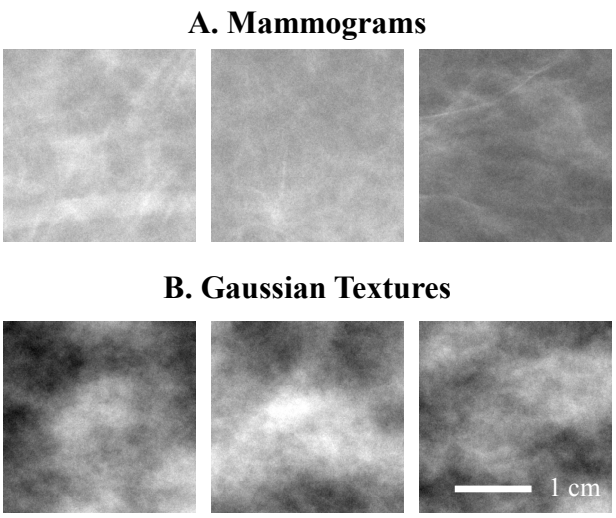

Figure 1. X-ray breast images and filtered noise. The upper panel of images (A) are taken from the interior of the left CC view from different patients. The images have been log-converted from the normalized detector outputs, but no further display processing has been applied. The lower panel of images (B) are the result of a Gaussian process with matched mean and power spectrum. A common intensity window is applied to all images.

Figure 1 suggests that if the statistical properties approach is going to be effective, we will likely need to evaluate properties beyond the mean and power spectrum that fully characterize a stationary Gaussian process. We consider these to be "non-Gaussian" statistics that assess relevant higher-order structure in the images. In this work we evaluate one such measure, known as the Laplacian Fractional Entropy (LFE), for this purpose [3]. LFE is based on response histograms of Gabor filters, which are intended to represent receptive fields in early visual cortex [4-6]. Similar to visual receptive fields, the measure can be tuned to different bandwidths, center-frequencies, phase, and orientations. The measure computes the entropy of the histogram relative to the histogram from a Gaussian process. This relative entropy will be zero when the two histograms match, making the measure insensitive to Gaussian statistics. The Laplacian distribution is used as a yardstick for measuring how much a response histogram deviates from Gaussian form. An LFE value of 100% is interpreted as being as non-Gaussian as a Laplacian distribution.

In this paper, we compare higher-order statistical properties of various virtual breast phantoms to a sample of patient mammograms. For reference we also compare the power-spectra. It is well known from the multiple studies [1, 2, 7] that power spectra of projection mammograms are well described by a power-law at low spatial frequencies where anatomical effects dominate. At higher frequencies, where noise is the dominant source of variability, the spectrum departs from the power-law.

2. MATERIALS AND METHODS

2.1 Mammograms

The mammograms we use were obtained from the UC Davis Medical Center under an IRB approved human-subjects protocol that included de-identifying the image data. Mammograms were acquired on a Hologic Dimensions system (Hologic Inc., Bedford MA). The images were saved in the pre-processed mode (i.e. "for processing") and converted to density by a log-transform. This step was done to avoid any non-Gaussian statistics that might be introduced by nonlinear transformations in the "for-display" processing. Pixel size in the mammograms was 100 microns. We use a total of 19 patient images that had a large enough central region (1024 by 1024 pixels) to assure that response histograms would not have excessive noise.

2.2 Clustered-Blob Lumpy Backgrounds

The Clustered-Blob Lumpy Backgrounds (CBLBs) have bend developed by Bochud and colleagues [8, 9] as an extension of Rolland and Barrett's Type I Lumpy backgrounds [10]. The idea behind lumpy backgrounds was that a background could be generated as a superposition of lump profiles placed at different locations throughout the background area. The CBLB extended this by allowing the lump profile to be a localized probability density for a cluster made up from smaller lumps.

A total of five CBLBs are considered here. These include the process described in the original publication [8] and referred to as OpExp99, as well as four virtual breast phantoms developed in a subsequent publication [9]. Two virtual phantoms based on oriented and isotropic processes are referred to as SimpOri and SimpIso respectively. The remaining two phantoms both sum two CBLB processes modeling glandular and fibrous structure. These also incorporate oriented and isotropic processes, and are referred to ad DoubOri and DoubIso. The parameters for these processes are all taken directly from the original publications, with the only change being to scale the number of clusters in the simulation by 16 to match the larger image size (1024 × 1024 instead of 256 × 256) tested. Figure 2 gives examples from each of these processes along with a power-law Gaussian texture for reference.

It should be noted that the CBLB phantoms directly simulate a 2D image. This is considerably simpler than the methods below, which simulate a 3D breast, and then project the 3D simulation onto a 2D detector.

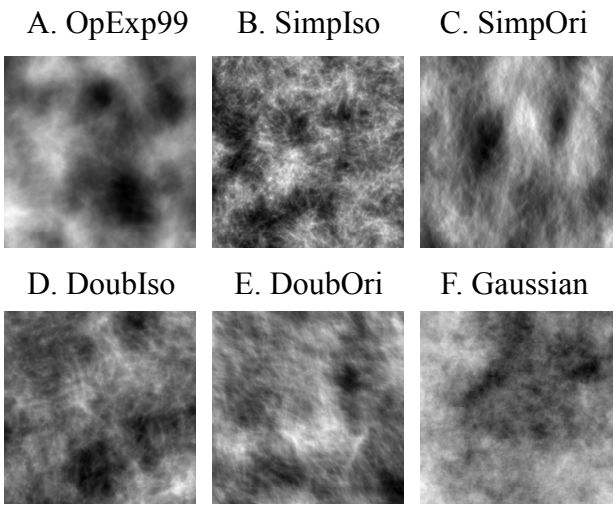

Figure 2. Examples of Clustered-Blob Lumpy Backgrounds. The images show 256 × 256 pixel samples from each of the five CBLB textures (A-E). A Gaussian texture with a power-law spectrum (F) is shown for reference.

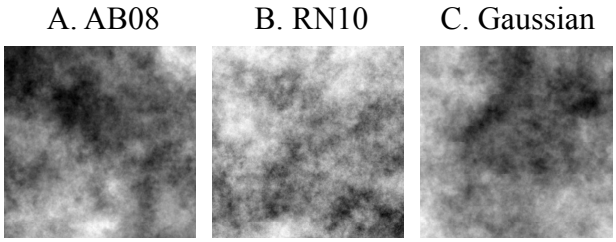

Figure 3. Examples of Truncated Binary Process Backgrounds. The images show examples using the approach of Abbey and Boone (A) and Reiser and Nishikawa (B). The processes have been integrated over a 5cm thickness, and converted from transmission to density. A Gaussian texture with a power-law spectrum (C) is shown for reference.

2.3 Truncated Binary Processes

The "binary-truncation" (BT) phantoms are based on the idea that the breast can be well modeled as mixture of adipose and glandular tissues, each characterized by its respective attenuation coefficient. These models have typically neglected calcifications. The spatial distribution of the attenuation coefficients is generated by thresholding a 3D random process. The approach of Abbey and Boone [11] (AB08) uses a 3D Gaussian process truncated to approximately 30% volume glandular fraction. Rieser and Nishikawa [12] (RN10) used phase randomization followed by thresholding to generate the distribution of adipose and glandular tissue and targeted a 75% glandular fraction. It should be noted that both of these approaches have somewhat higher glandular fractions than the 19% average volume glandular fraction of the breast as measured from dedicated breast CT images [13].

We used the procedures described in both publications [11, 12] to generate binary 3D backgrounds with an isotropic sampling of 100 μm. The grid was 1024 × 1024 × 512, and thus captured the 5cm average thickness of a compressed breast in a screening mammography exam. Phantoms were projected onto a 100 μm detector by summing the z-dimension of the 3D phantom. Examples of BT phantoms from these two processes are shown with a Gaussian power-law process as a reference in Figure 3.

2.4 The UPenn Virtual Breast Phantom

A virtual breast phantom has been under development at the University of Pennsylvania for several years [14-16]. This phantom is based on simulating the major anatomical components of the breast, including skin, adipose tissue, fibroglandular tissue, and Cooper's ligaments. The breast simulation is initially generated in an uncompressed state, to which a compression transform is applied using a finite element model.

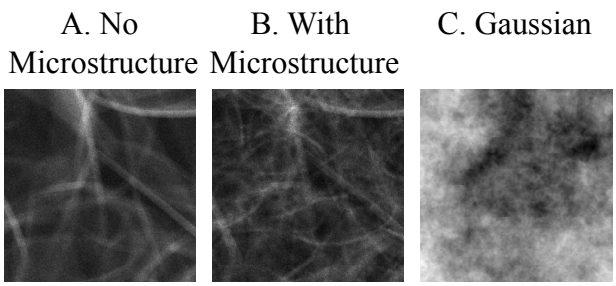

Figure 4. Examples of the UPenn Virtual Breast Phantom. The images show an example of the breast phantom being developed at the University of Pennsylvania (A) and a recent version that includes a model of breast microstructure (B). The backgrounds have been converted from transmission to density. A Gaussian texture with a power-law spectrum (C) is shown for reference.

We consider two versions of the UPenn phantom. The first is the published version of the phantom, tailored for projection mammography [15]. In the second version, a new approach currently under investigation was used that involved simulating additional microstructure in the adipose compartments. Mammograms were simulated from the 3D phantom assuming, a 950 mL breast volume with 6.4 cm compressed breast thickness, a polyenergetic x-ray beam, and 100 μm detector pixels. Examples images from these two phantoms are given in Figure 4.

2.5 Image Analysis

Gaussian white noise was added to the phantoms to simulate the effects of quantum and electronic acquisition noise. The magnitude of the noise was set to approximately equal the amplitude of anatomical noise at 1.0 cyc/mm, the spatial frequency at which the power spectrum begins to diverge from the power-law form. Figure 5 gives examples of the appearance of the phantom images after noise has been added.

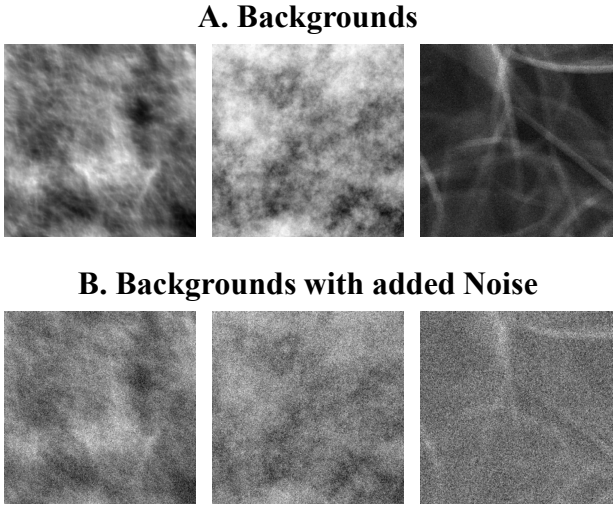

Figure 5. Addition of Acquisition noise. Example CBLB, TB and Upenn phantom images before and after the addition of noise. The magnitude of the noise was set to approximately equate power at 1 cyc/mm.

Power spectra were computed by sampling fifty 256 ×256 pixel ROIs at random from within the ROI of the images, These were mean subtracted and then windowed using a radially symmetric Hanning window that extended to the edge of the ROI [17]. The average of the squared magnitude of the Fourier Transform was taken as the estimate of the power spectrum for that image. Averages across images were used as the final estimate of the power spectrum.

The LFE was computed according to a recent publication [3]. Gabor filters that spanned center frequencies from 0.125 cyc/mm to 2.8 cyc/mm were evaluated at six different orientations. The filters were sine-phase with 1.4 octave bandwidth, and an aspect ratio of 1. Filter responses from 1cm inside the boundary of the ROI were used. The histograms binned the central 99% of the responses, with an additional 1% bin for the remaining extremal values.

3. RESULTS AND DISCUSSION

The main results of this work are power and LFE averaged over orientations and plotted as a function of spatial frequency (i.e. power spectra and LFE spectra).

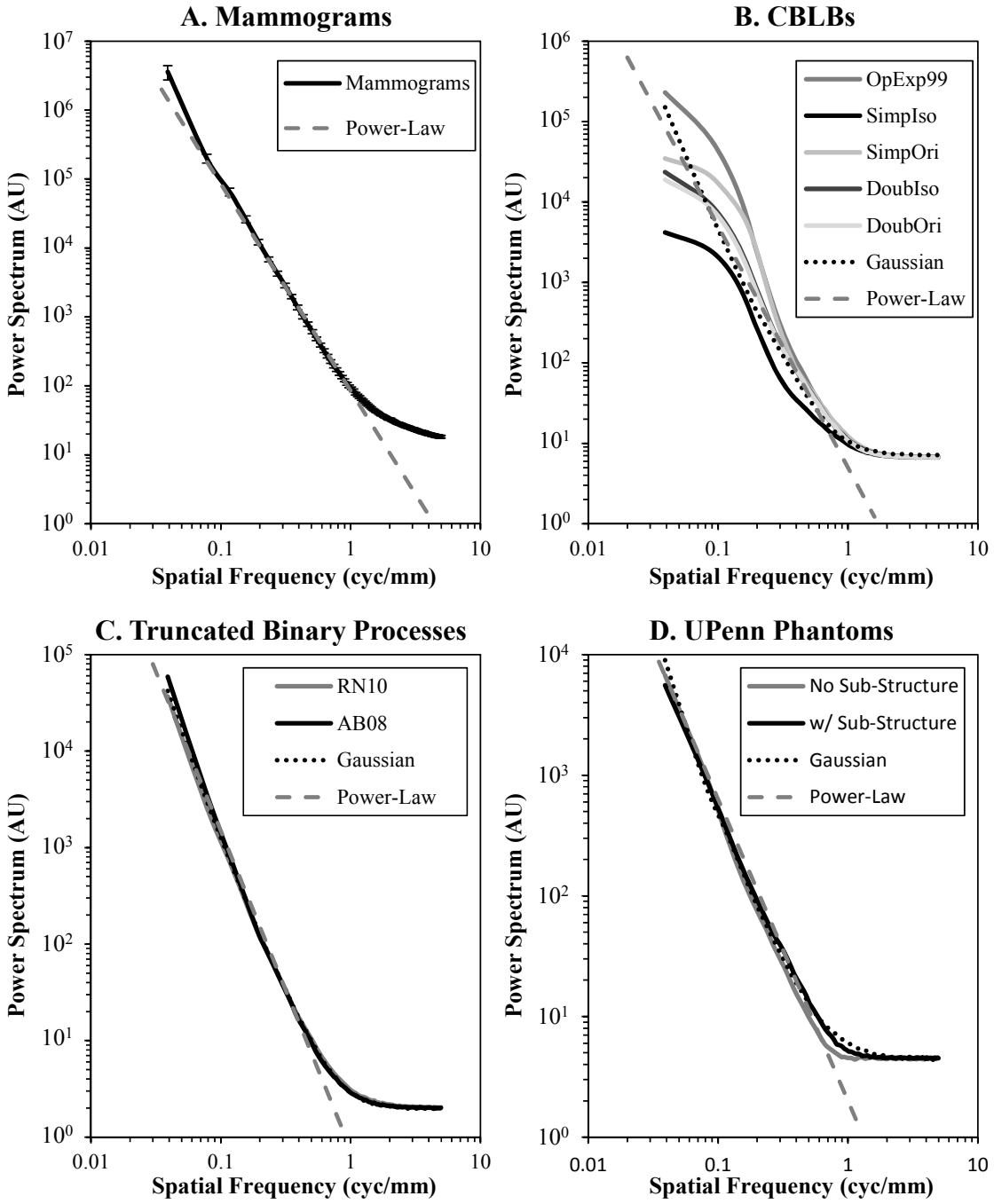

Figure 6. Power Spectra for Phantoms and Mammograms. Power spectra derived from the sample of mammograms (A) are shown along with the three classes of virtual breast phantoms (B-D). A line representing an ideal power-law is plotted in each case along with a Gaussian texture for each of the phantom classes.

3.1 Power Spectra

Figure 6 plots the power spectra for the mammograms and each of the virtual breast phantoms with added image noise. In each case, a fitted line representing a power-law power spectrum is plotted for reference. The mammography data in Figure 6A closely follow the power-law at low spatial frequencies until about 1.0cyc/mm . The exponent of this power law is 3.0. This is consistent with previous findings [1, 2].

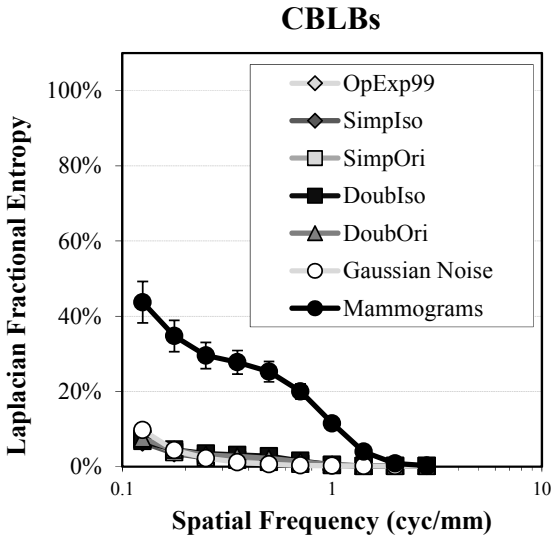

Figure 7. Laplacian Fractional Entropy for Clustered-Blob Lumpy Backgrounds. LFE is plotted as a function of spatial frequency for each of the five clustered-blob backgrounds, as well as a matched Gaussian noise texture. For reference the LFE from the sample mammograms is also plotted (error bars = ±1 std. err.).

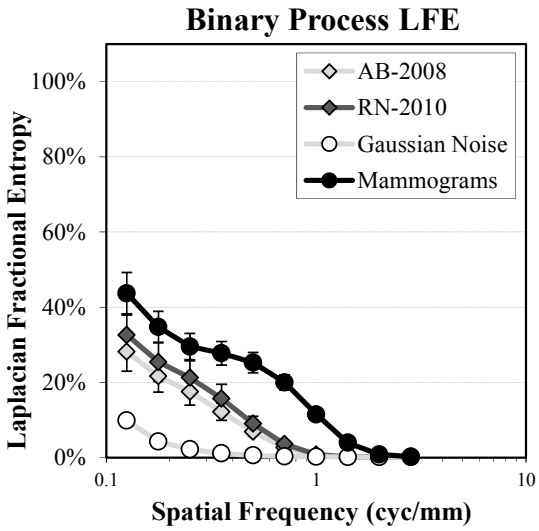

Figure 8. Laplacian Fractional Entropy for Truncated Binary Processes. LFE is plotted as a function of spatial frequency for both of the truncated binary backgrounds, as well as a matched Gaussian noise texture. LFE from the sample mammograms is also plotted (error bars = ±1 std. err.).

The CBLBs in Figure 6B appear to rolloff at the lowest spetial frequencies plotted, before adopting an approximately power-law form (exponent is 3.0) from 0.1 to 1.0 cyc/mm, and then departing from this as the contribution of noise increases at higher frequencies. Similar power-law evaluations of the CBLBs were made in the primary publications [8, 9], and the processes did not exhibit as much departure from the power law at low spatial frequencies. This may be due to differences in how the power spectra were computed, although further investigation of this difference is warranted.

The truncated binary processes in Figure 6C and the UPenn phantoms in Figure 6D are well approximated by power-laws at low spatial frequencies, with noise-induced departure beginning at 1cyc/mm. We note that the TB phantoms are fit by a power-law with an exponent of 3.3, and the UPenn phantom is fit by a power-law with exponent of 2.5.

Even with some departures at low-frequencies by the CBLBs, the general finding is that the power spectra of the virtual phantoms are reasonably well fit by a power-law over the frequencies in which anatomical variability dominates, even though the various phantoms have quite different visual appearances. This is a testament to the ubiquitous nature of the power law. However, when the goal is to distinguish between various models, the generality of the power law may work against its usefulness. This serves as the motivation for investigating higher-order statistical properties.

3.2 Laplacian Fractional Entropy

Figure 7 shows the LFE for the CBLBs, along with a matched Gaussian texture. Non zero LFE for the Gaussian texture reflects departures in the histogram due to the limited spatial extent of the ROI used to compute the histogram. Also plotted for reference is the LFE computed from the sample of mammograms. The mammograms start at an LFE of approximately 40% at the lowest spatial frequency measured (0.125 cyc/mm), and decrease at higher spatial frequencies nearing zero by about 2 cyc/mm, The Gaussian process starts at about 10% LFE and nearing zero by about 0.2 cyc/mm. Surprisingly, LFE is not substantially different from the matched Gaussian texture across frequencies.

Figure 8 shows LFE plots for the TB phantoms, along with a matched Gaussian texture and mammograms. The TB phantoms start at approximately 30% LFE at 0.125 cyc/mm, and decrease steadily nearing zero at 1.0

cyc/mm. While substantially greater than the Gaussian process, LFE from the TB processes is still substantially less than the average measured from mammograms.

Figure 9 Shows the LFE plots for the UPenn phantoms matched Gaussian texture, and mammograms. At low spatial frequencies, the UPenn phantom without additional microstructure was found to exceed the LFE of the mammograms, with peak LFE of 92% at 0.35 cyc/mm. After this peak, LFE dropped rapidly to zero at 1.0 cyc/mm. The addition of microstructure reduced LFE values, more closely matching the mammograms.

All of the virtual phantoms had dropped to values near zero by 1.0 cyc/mm, although the mammograms maintain non-zero LFE until closer to 2.0 cyc/mm. This may be a consequence of adding too much noise to the phantoms, thereby driving LFE to zero.

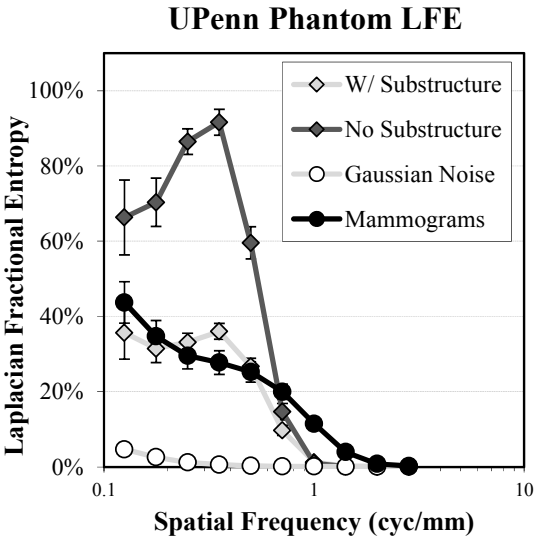

Figure 9. Laplacian Fractional Entropy for Upenn Phantoms. LFE is plotted as a function of spatial frequency for the Upenn phantom both with and without microstructure, as well as a matched Gaussian noise texture. LFE from the sample mammograms is also plotted (error bars = ±1 std. err.).

4. CONCLUSIONS

This study of three classes of virtual breast phantoms shows that all have power spectra that are qualitatively similar to the power-law form that has been used to describe projection mammograms by Bochud [1], Burgess [2], Heine [7, 18], and others. While this shows that the various phantoms have similar second-order statistical properties to clinical breast images, it also illustrates the limitations of the power spectrum for discriminating between phantoms. The similarity of the phantoms at the level of the power-spectrum indicates the importance of higher-order structure in the appearance and realism of virtual breast phantoms.

By contrast, Laplacian Fractional Entropy is insensitive to the power spectrum of the phantoms. Instead, this measure focuses on non-Gaussian statistical properties in the response histograms of Gabor filters intended to represent receptive fields in early visual cortex. Aside from Gaussian processes used as a reference, all of the breast phantoms considered here are rigorously non-Gaussian in that their probability distributions depart from that of a multivariate Gaussian process. The LFE can be thought of as one possible measure of the degree of this departure. By this measure we find substantial differences between the different classes of breast phantoms. The clustered-blob lumpy backgrounds have modest values of LFE, less than 10% across spatial frequencies from 0.125 cyc/mm to 2.8 cyc/mm. Binary truncation processes are somewhat higher, but are still uniformly less than the sample of mammograms. The UPenn Virtual Breast Phantom has considerably higher LFE, and the addition of microstructure results in an LFE that is closer to the mammograms.

It is our belief that these examples suggest and partially illustrate the role of higher-order statistical properties in validating the realism of virtual breast phantoms.

ACKNOWLEDGEMENTS

Dr.s Abbey and Boone were partially supported by US National Institutes of Health (R01-EB002138). Dr.s Abbey and Eckstein was partially supported by US National Institutes of Health (R01-EY015925) and the U.S. Army Research Office (W911NF-09-0001). Dr.s Bakic, Pokrajac, and Maidment have been partially supported by US National Institutes of Health (R01-CA154444 and R21-CA155906), the US Department of Defense Breast Cancer Research Program (HBCU Partnership Training Award BC083639 and grants 45395-MA-ISP, #54412-CI-ISP, W911NF-11-2-0046), and the US National Science Foundation (CREST: HRD-0630388 and III-0916690). The content is solely the responsibility of the authors and does not necessarily represent the views of these funding agencies.

REFERENCES

[1] F. O. Bochud, F. R. Verdun, C. Hessler, and J. F. Valley, "Detectability of radiological images: The influence of anatomical noise," *Proc. SPIE*, 2436, 156-164 (1995).

[2] A. E. Burgess, F. L. Jacobson, and P. F. Judy, "Human observer detection experiments with mammograms and power-law noise," *Med Phys,* 28, 419-37 (2001).

[3] C. K. Abbey, A. Nosrateih, J. Sohl-Dickstein, K. Yang, and J. M. Boone, "Non-Gaussian statistical properties of breast images," *Med Phys,* 39, 7121-30 (2012).

[4] R. L. De Valois, D. G. Albrecht, and L. G. Thorell, "Spatial frequency selectivity of cells in macaque visual cortex," *Vision Res,* 22, 545-59 (1982).

[5] D. J. Field, "Relations between the statistics of natural images and the response properties of cortical cells," *J Opt Soc Am A,* 4, 2379-94 (1987).

[6] D. L. Ringach, M. J. Hawken, and R. Shapley, "Receptive field structure of neurons in monkey primary visual cortex revealed by stimulation with natural image sequences," *J Vis,* 2, 12-24 (2002).

[7] J. J. Heine, S. R. Deans, D. K. Cullers, R. Stauduhar, and L. P. Clarke, "Multiresolution statistical analysis of high-resolution digital mammograms," *IEEE Transactions on Medical Imaging,* 16, 503-515 (1997).

[8] F. Bochud, C. Abbey, and M. Eckstein, "Statistical texture synthesis of mammographic images with super-blob lumpy backgrounds," *Opt Express,* 4, 33-42 (1999).

[9] C. Castella, K. Kinkel, F. Descombes, M. P. Eckstein, P. E. Sottas, F. R. Verdun, and F. O. Bochud, "Mammographic texture synthesis: second-generation clustered lumpy backgrounds using a genetic algorithm," *Opt Express,* 16, 7595-607 (2008).

[10] J. P. Rolland and H. H. Barrett, "Effect of random background inhomogeneity on observer detection performance," *J Opt Soc Am A,* 9, 649-58 (1992).

[11] C. K. Abbey and J. M. Boone, "An ideal observer for a model of x-ray imaging in breast parenchymal tissue," *Proceedings of IWDM*, 5116, 393-400 (2008).

[12] I. Reiser and R. M. Nishikawa, "Task-based assessment of breast tomosynthesis: effect of acquisition parameters and quantum noise," *Med Phys,* 37, 1591-600 (2010).

[13] M. J. Yaffe, J. M. Boone, N. Packard, O. Alonzo-Proulx, S. Y. Huang, C. L. Peressotti, A. Al-Mayah, and K. Brock, "The myth of the 50-50 breast," *Med Phys,* 36, 5437-43 (2009).

[14] P. R. Bakic, M. Albert, D. Brzakovic, and A. D. Maidment, "Mammogram synthesis using a 3D simulation. I. Breast tissue model and image acquisition simulation," *Medical Physics,* 29, 2131-2139 (2002).

[15] P. R. Bakic, C. Zhang, and A. D. Maidment, "Development and characterization of an anthropomorphic breast software phantom based upon region-growing algorithm," *Medical Physics,* 38, 3165-76 (2011).

[16] D. D. Pokrajac, A. D. Maidment, and P. R. Bakic, "Optimized generation of high resolution breast anthropomorphic software phantoms," *Medical Physics,* 39, 2290-302 (2012).

[17] K. G. Metheany, C. K. Abbey, N. Packard, and J. M. Boone, "Characterizing anatomical variability in breast CT images," *Med Phys,* 35, 4685-94 (2008).

[18] J. J. Heine, S. R. Deans, R. P. Velthuizen, and L. P. Clarke, "On the statistical nature of mammograms," *Med Phys,* 26, 2254-65 (1999).

Realistic Simulation of Breast Tissue Microstructure in Software Anthropomorphic Phantoms

Predrag R. Bakic,[1] David D. Pokrajac,[2]
Raffaele De Caro,[3] and Andrew D.A. Maidment[1]

[1] Dept. of Radiology, University of Pennsylvania, Philadelphia, PA, USA
[2] Computer and Information Sciences Dept., Delaware State University, Dover, DE, USA
[3] Dept. of Human Anatomy and Physiology, University of Padova, Italy
Predrag.Bakic@uphs.upenn.edu

Abstract. Software anthropomorphic breast phantoms have been used in virtual clinical trials for preclinical validation of breast imaging systems. Virtual trial quality depends largely on the realism of the simulated breast anatomy. Our phantom design has been focused on the simulation of large-scale and meso-scale anatomical structures, including the breast outline, skin, and matrix of Cooper's ligaments and tissue compartments. Realism of such a design has been confirmed in comparative studies of phantom and clinical power spectra and parenchymal texture. We present a novel method for simulating the hierarchical organization of breast tissue subcompartments, seen in detailed histological images. The subcompartmentalization introduces microstructure in breast phantoms, resulting in improved realism of phantom images. The qualitative validation of phantoms with simulated microstructure is discussed in this paper; the quantitative validation in ongoing.

Keywords: Software breast phantoms, virtual clinical trials, small-scale tissue simulation, stereology, testing realism.

1 Introduction

Virtual clinical trials (VCTs) have received considerable attention recently; a VCT is an efficient way to perform optimization and preclinical validation of novel breast imaging systems (1, 2). VCTs are based upon sophisticated computer simulations of breast anatomy, image acquisition, image processing and display. The synthetic images generated by VCT can be assessed by model or human observers.

The quality of a VCT depends upon a number of factors including phantom realism; the phantom realism needs to be commensurate with the diagnostic task in question. The University of Pennsylvania (UPenn) breast anatomy model is based upon the simulation of large-scale and meso-scale anatomical structures; a variety of features are modelled, including the overall breast outline, the skin, the matrix of Cooper's ligaments and tissue compartments, and the assignment of adipose and fibroglandular tissue to these compartments.(3) The validity of this design has been confirmed for a number of tasks, and the visual realism of the anatomy model is

H. Fujita, T. Hara, and C. Muramatsu (Eds.): IWDM 2014, LNCS 8539, pp. 348–355, 2014.

supported by a number of comparative studies of phantom and clinical power spectra (4, 5) and parenchymal texture (6-8).

That said, we are constantly striving to improve the breast anatomy model further. In this paper, we present a novel method for simulating the hierarchical organization of breast tissue subcompartments, seen in detailed histological images. The introduction of a hierarchy of subcompartments into our breast anatomy model results in more realistic phantom images.

2 Methods

2.1 Histological Analysis

Our existing method for simulating breast tissue structures was motivated by the observed appearance of tissue compartments in existing histology and computed tomography breast images. In this paper we present a new analysis of histology slices from two breasts specimens; one obtained after breast reduction and another after mastopexy. The patients were aged 33 and 50, respectively. No abnormalities were detected in the two analysed breast specimens. The histologic analysis was performed at the University of Padova, Italy. Ten histology slices were analysed, at least one slice from each breast quadrant.

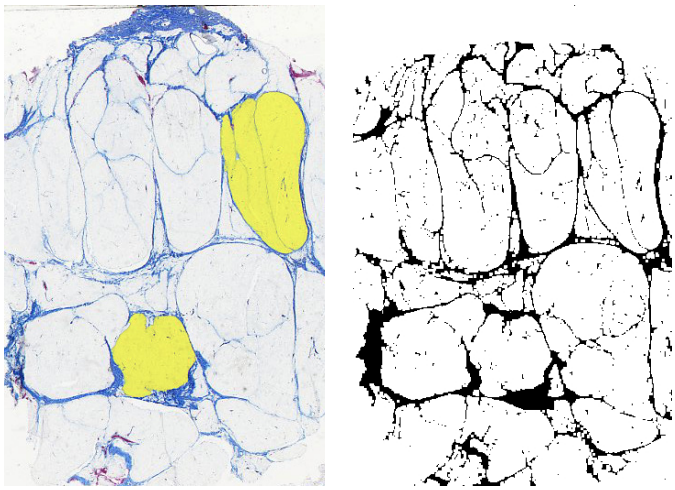

(a) (b)

Fig. 1. An example of a breast histology image used in the size and shape analysis of adipose tissue compartments: (a) histology section with the Azan-Mallory staining; two analysed compartments are highlighted; (b) a binarized version of the same histology section

Fig. 1(a) shows a detailed microscopic image of the breast obtained using Azan-Mallory staining. The Azan-Mallory staining technique combines the original Mallory

connective tissue stain with azocarmine (9); as a result, collagen is stained blue, nuclei and cytoplasm are red, and elastic fibres are pink or unstained. The section in Fig. 1(a) is oriented so that the areolar region is superior. In this example, the adipose tissue compartments are clearly encapsulated by the blue stained Cooper's ligaments. Two individual compartments have been highlighted to illustrate this observation.

Digital images of the stained histologic slices were binarized by thresholding. A binarized image of the matching tissue section is shown in Fig. 1(b). The binarized sections were used to estimate the size and shape of the tissue compartments. Two parameters, mean volume and axial ratio, were calculated using the stereological unfolding method by Saltykov, which assumes an ellipsoidal compartment shape (10). From this, compartment size and shape distributions were calculated.

Examination of Fig. 1 suggests that the thickness of the Cooper's ligaments depends upon the volume of the associated compartments. Thus, we have also estimated the volumetric fraction of the connective tissue and the average thickness of the Cooper's ligaments.

Finally, as seen in Fig. 1(a), the individual adipose compartments appear to be divided into smaller compartments by interlobular fibrous septa. Due to their small thickness, these interlobular fibrous septa may not be clearly visible in clinical breast images; however, they certainly contribute to the small-scale tissue variations seen in clinical images. The combination of the thicker Cooper's ligaments and the thinner interlobular fibrous septa indicate a hierarchical organization of tissue compartments. This observation has motivated the modification of our breast anatomy model.

2.2 Computer Simulation

In order to increase the realism of our breast anatomy model, we have included a simulation of subcompartments with septa of reduced thickness. We begin by simulating a baseline phantom, *P*, containing large compartments and correspondingly thick ligaments. We then simulate a second subcompartment phantom, *S*, having the same size and outline as the baseline phantom, containing smaller compartments and thinner ligaments; the internal structure of the second phantom will form the structure of the subcompartments. The final phantom is obtained by superimposing the subcompartment phantom on the baseline phantom. Algorithmically, a voxel $v_p(x,y,z)$ of *P* at spatial coordinate x,y,z is replaced by the corresponding voxel $v_s(x,y,z)$ of *S* if and only if $v_s(x,y,z)$ is part of a ligament in S, and $v_p(x,y,z)$ belongs to a compartment in P.

We tested this method with a set of preliminary models in which each compartment in *P* was divided on average into thirty subcompartments. In this test, we simulated baseline phantoms with 333 compartments and subcompartment phantoms with 10,000 compartments. The simulated thickness of the interlobular fibrous septa was selected to be 200μm in the subcompartment phantoms, 3 times smaller than the 600μm thickness of the primary Cooper's ligaments in the baseline phantoms.

The simulated microstructure was assessed subjectively based upon synthetic mammographic projections of phantoms with or without subcompartments. The synthetic images were generated using the breast anatomy and imaging simulation

pipeline, developed at the University of Pennsylvania for the purpose of conducting VCTs of breast imaging systems (1). The pipeline includes modules for the simulation of normal breast anatomy, insertion of lesions, breast positioning and deformation, clinical image acquisition, image reconstruction and post-processing, image display, and image interpretation by model observers. External modules may be included in the pipeline as plugins.

The software breast phantoms with and without subcompartments were subject to simulated mammographic compression using a finite element deformation method (11). Mammographic imaging was then simulated using a ray tracing projection method, assuming a poly-energetic x-ray beam without scatter, and an ideal detector model. The quantum noise was simulated by adding a random Poisson process. The simulated image acquisition geometry corresponds to the Hologic Selenia Dimensions full-field digital mammography system (Hologic Inc., Bedford, MA). The resulting synthetic raw projections are post-processed using a commercial software package (Adara, Real Time Tomography, Villanova, PA).

3 Results and Discussion

3.1 Histological Analysis

Table 1 gives the values of average compartment volume, axial ratios and ligament thickness, as estimated from histology slides, in three different regions of the breast: subcutaneous ("Sub-Q"), posterior, and periglandular. These values have been averaged over 30 analysed adipose compartments. Adipose tissue compartments have a larger volume in the subcutaneous (0.84 ml) and posterior (0.94 ml) regions, as compared to the periglandular region (0.26 ml). Visually, these estimates of compartment volume agree with the observed appearance of breast tissue structures in these regions of clinical images.

The orientation of the breast tissue compartments had relatively little dependence upon region; the axial ratio varied from 2.02 in the subcutaneous region to 2.91 in the posterior region. This range of axial ratios corresponds to an angular difference of just 7 degrees. The variation in angular ratios is considerably larger in the posterior region (0.30; i.e., 10% of the average angular ratio), as compared to the subcutaneous region (0.14; 6%) and periglandular region (0.12; 6%). This suggests that some underlying structure may exist in these areas, which constrains the shape and orientation of the compartments.

Table 2 shows the volume fraction and thickness of the connective tissue, estimated from the binarized images of the stained Cooper's ligaments. The tabulated values have been averaged over 10 analysed tissue slices. The estimated average volume fraction was 12.3%, while the average thickness of Cooper's ligaments was 289 μm. The estimated ligament thickness fits well within the range of thicknesses used in our previous computer simulation of Cooper's ligaments: 200-600 μm. The volume fraction showed 11% variation relative to the mean value, while the ligament thickness showed 5% variation relative to the mean value.

Table 1. Average values of compartment volumes and axial ratios in various breast regions, estimated from breast histological sections

Region	Volume (cm^3)	Axial ratio
Sub-Q	0.84 ± 0.04	2.02 ± 0.14
Posterior	0.94 ± 0.07	2.91 ± 0.30
Periglandular	0.26 ± 0.01	2.04 ± 0.12

Table 2. Average values of the connective tissue volume fraction and thickness, estimated from Cooper's ligaments in breast histological sections

	Volume fraction (%)	Thickness (μm)
Cooper's ligaments	12.3 ± 1.4	289.2 ± 13.0

3.2 Computer Simulation

Fig. 2 shows preliminary results of the simulation of subcompartments in a breast phantom. Fig. 2(a) show a cross-section of a baseline phantom simulated with

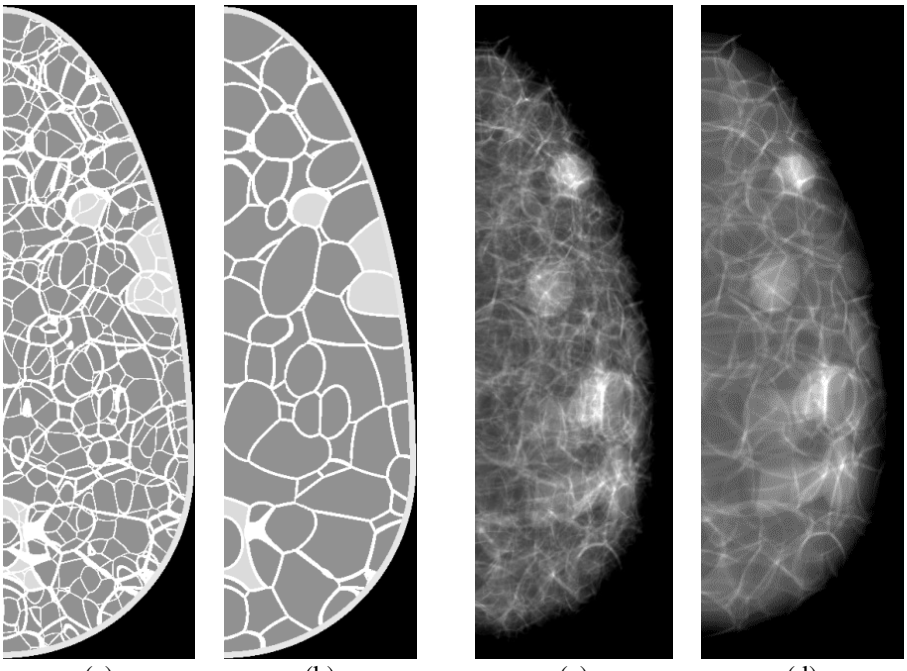

(a) (b) (c) (d)

Fig. 2. Simulation of breast tissue microstructure by subcompartmentalization. Shown are sections of a software phantom (a) with and (b) without subcompartments, with corresponding synthetic mammographic projections (c) with and (d) without subcompartments.

subcompartments, while Fig. 2(b) shows the same phantom without subcompartments. Figs. 2(c-d) show the corresponding synthetic mammographic projections of these phantoms. In both cases, the phantoms have a total volume of 450 cm^3, with 100 μm voxels. Subjectively, the projection image of the subcompartmentalized phantom shows a higher level of realism. The simulated parenchymal pattern is enriched by the addition of small-scale structures. In addition, the simulated Cooper's ligaments appear less prominent and less geometric, as compared to the projection of the phantom without subcompartments.

A quantitative analysis was performed by comparison of the Laplacian Fractional Entropy (LFE) in clinical and synthetic images. The LFE measure describes the relative content of non-Gaussian statistics in breast images (12). The LFE analysis of the phantoms confirmed that the addition of subcompartments yields a considerable improvement in the LFE measure; the phantom with subcompartments is much closer to clinical images (8). The results of the LFE analysis are shown in Fig. 3. At low spatial frequencies, the phantom without subcompartments exceeds the LFE estimated in clinical mammograms. The peak LFE value of 92% occurs at 0.35 cyc/mm. At spatial frequencies above this peak, the LFE drops to zero at 1.0 cyc/mm. Subcompartmentalization reduces the LFE values, thus matching closely those estimated in mammograms. Based upon our current simulation method, subcompartmentalization increases the simulation time proportional to the square root of the number of compartments. This may be potentially prohibitive for real-time VCT simulations. As a viable alternative, we could pre-compute a number of subcompartment phantoms to be combined randomly with baseline phantoms created in real time.

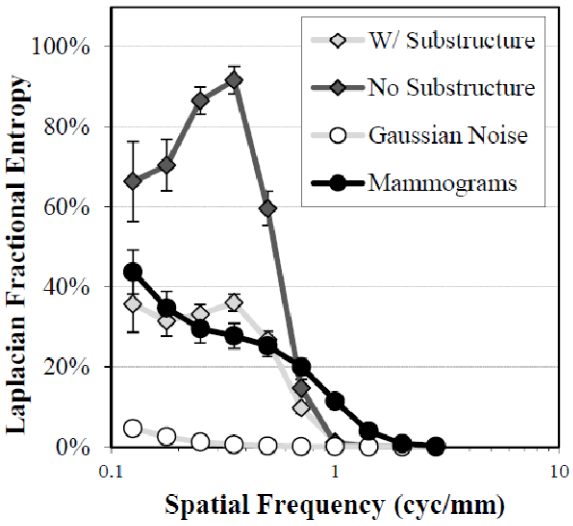

Fig. 3. Laplacian Fractional Entropy (LFE) as a function of spatial frequency, estimated from phantoms generated with and without subcompartments. The phantom LFE values are shown in comparison with those estimated from clinical mammograms and simulated Gaussian noise. Error bars show ±1 standard deviation. (Reproduced with permission from Ref. #8.)

Our future work will include a more detailed analysis of phantoms containing subcompartments, and a more complete exploration of the various simulation parameters for each of the tissue regions analysed in this work (subcutaneous, deep, and periglandular). In this way, we hope to add spatial dependence to our anatomy simulation method, further improving realism.

4 Conclusions

We have simulated the microstructure of breast tissue by adding subcompartments to our current design of anthropomorphic breast phantoms. This modification was motivated by the hierarchical organization of Cooper's ligaments and interlobular fibrous septa, as shown by Azan-Mallory stained breast histologic slices.

Subjectively, synthetic images of phantoms with subcompartmentalization show an improved level of realism; the simulated parenchymal pattern has been enriched, while the simulated Cooper's ligaments appear less geometric. The observed improvement in the appearance of phantom images is in agreement with a preliminary quantitative validation based upon Laplacian Fractional Entropy analysis.

Acknowledgements. This work was supported in part by the US National Institutes of Health (R01 grant #CA154444), the US Department of Defense Breast Cancer Research Program (HBCU Partnership Training Award #BC083639), the US National Science Foundation (CREST grant #HRD-0630388 and III grant # 0916690), and the US Department of Defense/Department of Army (45395-MA-ISP, #54412-CI-ISP, W911NF-11-2-0046), and the Delaware IDeA Network of Biomedical Research Excellence award. The content is solely the responsibility of the authors and does not necessarily represent the official views of the NIH, NSF and DoD. The authors are thankful to Drs. Veronica Macchi, Andrea Porzionato, and Cesare Tiengo from the University of Padova for preparing histological breast slides and performing the stereological analysis, and to Ms. Susan Ng from Real-Time Tomography (Villanova, PA) for processing simulated projection images. ADAM is a scientific advisor to Real-Time Tomography.

References

1. Maidment, A.D.A., Bakic, P.R., Chui, J.H., Avanaki, A.N., Marchessoux, C., Pokrajac, D.D., et al.: The Role of Virtual Clinical Trials in Preclinical Testing of Breast Imaging Systems. In: 99th RSNA Scientific Assembly and Annual Meeting. RSNA, Chicago (2013)
2. Bakic, P.R., Myers, K.J., Reiser, I., Kiarashi, N., Zeng, R.: Virtual Tools for Validation of X-Ray Breast Imaging Systems. Medical Physics 40(6), 390 (2013)
3. Pokrajac, D.D., Maidment, A.D.A., Bakic, P.R.: Optimized generation of high resolution breast anthropomorphic software phantoms. Medical Physics 39(4), 2290–2302 (2012)
4. Bakic, P.R., Lau, B., Carton, A.-K., Reiser, I., Maidment, A.D.A., Nishikawa, R.M.: An Anthropomorphic Software Breast Phantom for Tomosynthesis Simulation: Power Spectrum Analysis of Phantom Projections. In: Martí, J., Oliver, A., Freixenet, J., Martí, R. (eds.) IWDM 2010. LNCS, vol. 6136, pp. 452–458. Springer, Heidelberg (2010)

5. Lau, A.B., Bakic, P.R., Reiser, I., Carton, A.-K., Maidment, A.D.A., Nishikawa, R.M.: An Anthro-pomorphic Software Breast Phantom for Tomosynthesis Simulation: Power Spectrum Analysis of Phantom Reconstructions. Medical Physics 37, 3473 (2010)
6. Kontos, D., Bakic, P.R., Carton, A.-K., Troxel, A.B., Conant, E.F., Maidment, A.D.A.: Parenchymal Pattern Analysis in Digital Breast Tomosynthesis: Towards Developing Imaging Biomarkers of Breast Cancer Risk. Academic Radiology 16(3), 283–298 (2008)
7. Bakic, P.R., Keller, B., Zheng, Y., Wang, Y., Gee, J.C., Kontos, D., et al.: Testing Realism of Software Breast Phantoms: Texture Analysis of Synthetic Mammograms. In: Nishikawa, R.M., Whiting, B.R., Hoeschen, C. (eds.) SPIE Physics of Medical Imaging, vol. 8668. SPIE, Lake Buena Vista (2013)
8. Abbey, C.K., Bakic, P.R., Pokrajac, D.D., Maidment, A.D.A., Eckstein, M.P., Boone, J.M.: Non-Gaussian Statistical Properties of Virtual Breast Phantoms. In: Mello-Thoms, C.R., Kupinski, M.A. (eds.) SPIE Image Processing, Observer Performance, and Technology Assessment. SPIE, San Diego (2014)
9. Bergman, R.A.: Anatomy Atlases; A digital library of anatomy information, `http://www.anatomyatlases.org/` (cited March 8, 2014)
10. Weibel, E.R.: Stereological Methods. Academic Press, London (1979)
11. Lago, M.A., Maidment, A.D.A., Bakic, P.R.: Modelling of mammographic compression of anthropomorphic software breast phantom using FEBio. In: Int'l Symposium on Computer Meth-ods in Biomechanics and Biomedical Engineering. UT 2013, Salt Lake City (2013)
12. Abbey, C.K., Nosrateih, A., Sohl-Dickstein, J., Yang, K., Boone, J.M.: Non-Gaussian statistical properties of breast images. Medical Physics 39, 7121–7130 (2012)

Correlation between Topological Descriptors of the Breast Ductal Network from Clinical Galactograms and Texture Features of Corresponding Mammograms

Predrag R. Bakic[1], David D. Pokrajac[2], Mathew Thomas[1], Angeliki Skoura[3], Tatyana Nuzhnaya[4], Vasileios Megalooikonomou[3,4], Brad Keller[1], Yuanjie Zheng[1], Despina Kontos[1], James C. Gee[1], Gilda Cardenosa[5], and Andrew D.A. Maidment[1]

[1] Dept. of Radiology, University of Pennsylvania, Philadelphia, PA, USA
[2] Computer and Information Sciences Dept., Delaware State University, Dover, DE, USA
[3] Computer Engineering and Informatics Dept., University of Patras, Greece
[4] Computer and Information Science Dept., Temple University, Philadelphia, PA, USA
[5] Dept. of Radiology, Virginia Commonwealth University, Richmond, VA, USA
Predrag.Bakic@uphs.upenn.edu

Abstract. Mammographic texture has been reported as a biomarker of cancer risk. Recent publications also suggest correlation between the topology of the breast ductal network and risk of cancer. The ductal network can be visualized by galactography, the preferred imaging technique for nipple discharge. We present current results about the correlation between topological and textural properties of clinical breast images. This correlation was assessed for 41 galactograms and 56 mammograms from 13 patients. Topology was characterized using feature extraction techniques arising from text-mining, validated previously in the classification of normal, benign, and malignant galactograms. In addition, we calculated 26 texture descriptors using an automated breast image analysis pipeline. Regression analysis was performed between texture and topological descriptors averaged over all images of the same patient. These data demonstrate a correlation between topology and a subset of texture features with borderline statistical significance due to the limited sample size.

Keywords: Texture analysis, topology descriptors, galactograms, mammograms.

1 Introduction

Previously, we analysed the topological properties of the branching network of breast ducts as visualized by galactography, an x-ray imaging procedure of the contrast-enhanced breast ductal network (1-3). That analysis suggested a correlation between cancer risk and ductal network topology; this correlation also has been supported by evidence from murine cancer models (4). Clinical visualization of breast ducts is, however, not routinely performed; galactography is indicated infrequently, and it mostly commonly reveals benign findings (5, 6).

H. Fujita, T. Hara, and C. Muramatsu (Eds.): IWDM 2014, LNCS 8539, pp. 658–665, 2014.

On the other hand, texture descriptors of breast parenchyma are known to correlate with cancer risk (7-9). Our work is motivated by a desire to determine whether there is an association between parenchymal texture descriptors and ductal topology. Such an analysis would lead to improved models of breast anatomy, and may lead to a better understanding of breast cancer risk. Currently, breast cancer risk is estimated using patient demographic information and parenchymal texture features extracted from 2D mammograms. The spatial arrangement of breast tissue is, however, three-dimensional, stressing the need to understand the relationship between parenchymal structure and image texture.

The UPenn X-ray Physics Lab has extensive experience with the simulation of breast anatomy and imaging (10, 11). The development of the UPenn breast phantom is predicated upon a set of anatomically justified elements. To that end, we have chosen not to model the parenchymal texture by a random field with statistical properties similar to clinical data. This development process has been incremental, and continues to this day. For example, we have just recently begun to model the hierarchical organization of Cooper's ligaments seen in breast histology slices. A preliminary validation of a model of this small scale tissue detail, published separately in this proceedings, indicates good agreement with clinically estimated texture (12).

This paper presents our current results about the correlation between the ductal topology of clinical galactograms and the parenchymal textural properties of clinical mammograms from the same group of women. Understanding the relationship between mammographic texture and spatial distribution of breast anatomy will help optimize and extend our fully automated software pipeline for breast anatomy and imaging simulation; ultimately, we would like to be able to simulate specific cohorts of women, stratified by age, risk, and other factors.

2 Methods

2.1 Topological Analysis of Galactograms

In this paper, we analysed images of existing, anonymized clinical galactograms of 49 women, obtained from Virginia Commonwealth University. The data collection was performed after IRB review and was HIPAA compliant. Clinical galactograms were digitized from film, and categorized based upon the visibility of the ductal network. Ductal trees were traced manually from galactograms, followed by Prufer encoding of the breadth-first labelled ductal tree nodes (3). Then tf-idf significance weighting (3), originally used in text mining, was performed on the traced and encoded ductal trees. After manually tracing the ductal networks, a subset of 41 galactograms from 13 patients with well-defined ductal trees was selected for further processing and testing.

2.2 Texture Analysis of Mammograms

We measured 26 texture features in 56 digitized mammograms from the 13 selected patients imaged at Virginia Commonwealth University. Texture analysis was performed

using a fully automated software pipeline which extracted a large set of image features from the digitized mammograms (13). The pipeline calculates texture feature maps at points on a regular spatial lattice, determined by two parameters: the window size and the lattice distance. Here we use a window size of 63 pixels, and a lattice distance of 31 pixels. The analysed features are organized into three groups, including (i) descriptors of grey-level histograms, (ii) co-occurrence features, and (iii) run length features. These texture features have been used previously in breast cancer risk assessment studies (9). For the correlation analysis, the texture feature maps were averaged over the whole breast region (excluding the pectoral muscle and air).

2.3 Hypothesis Testing

We tested the hypothesis that there is a correlation between mammographic texture features and ductal topology descriptors. To that end, we have calculated the linear regression (14). The goal was to predict values of texture features averaged over all mammograms of the same patient as a function of the topological properties estimated from the corresponding manually-traced ductal networks, averaged over all galactograms of the same patient. Prior to the regression analysis, we combined the tf-idf topological descriptors via principal component analysis (PCA). The regression model considered the first 13 PCA components and the 26 texture features.

2.4 Power Calculations

It can be demonstrated that a small sample size (in this case 13 patients), could lead to large estimated p-values and hence rejection of valid linear regression models (large Type II error). To demonstrate the effect of sample size, we simulated an augmented dataset by bootstrapping (15). The bootstrapping was performed by replicating data records, with added Gaussian noise, for each PCA attribute and response variable. The standard deviation of the noise was 50% of the estimated standard deviation of the attributes or response variables.

3 Results and Discussion

Fig. 1 shows an example of a clinical galactogram used in this study (Fig. 1(a)), and the corresponding manually-traced ductal tree (Fig. 1(b)). The Prufer encoding and the tf-idf weights corresponding to the traced tree is also given (Fig. 1(c-d)). The example shown illustrates a breast with a malignant finding. Fig. 2 shows an example of a clinical mammogram from the same woman (Fig. 2(a)) and the corresponding texture feature map (Fig. 2(b)). Shown in this example, is a map of the entropy texture feature.

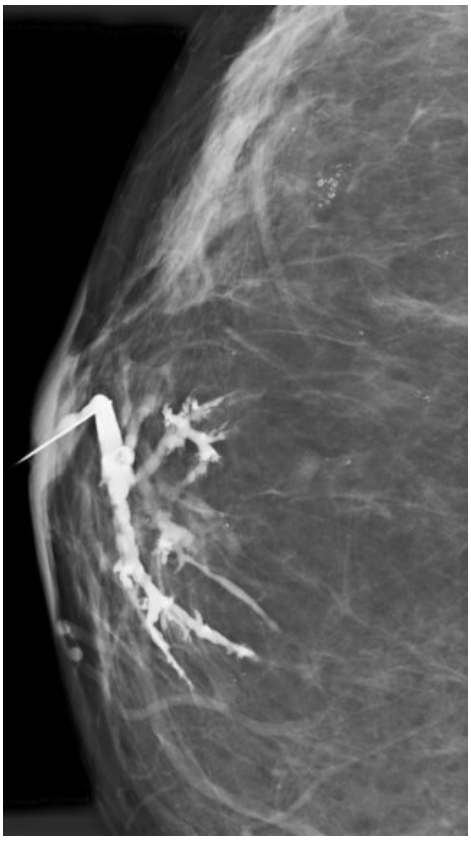

(a)

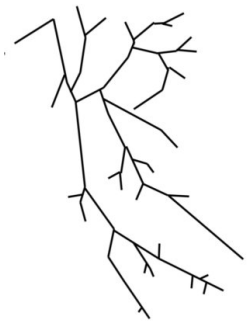

(b)

```
[ 1  1  3  4  6 10 10  6 11 16 16 11 17 24 24 17 25 34
 34 47 50 50 47 25  4  7 12 18 26 26 18 27 38 38 49 49
 27 12  7 13 20 28 28 20 29 29 13 21 30 30 21  3  5  5]
```

(c)

```
[0.00 0.11 0.45 0.36 0.40 0.50 0.71 0.00 0.50 0.77
 1.04 0.77 0.97 1.11 0.83 0.00 0.00 1.04 1.55 1.27
 1.45 1.19 0.00 0.00 1.27 0.00 0.00 0.00 0.00 0.00
 0.00 1.27 0.00 0.00 1.66 1.55 0.00 0.00 1.55 0.00
 0.00 1.45 0.00 2.04 2.19 1.66 0.00 1.90 0.00 0.00
 2.19 0.00 0.00 0.00 0.00 1.55 0.00 0.00 0.00 3.36]
```

(d)

Fig. 1. Illustration of the topological descriptors of the breast ductal network. Shown are: (a) a clinical galactogram with malignant finding; (b) the corresponding manually-traced ductal tree; (c) the Prufer encoding; and (d) the tf-idf weights corresponding to the ductal tree.

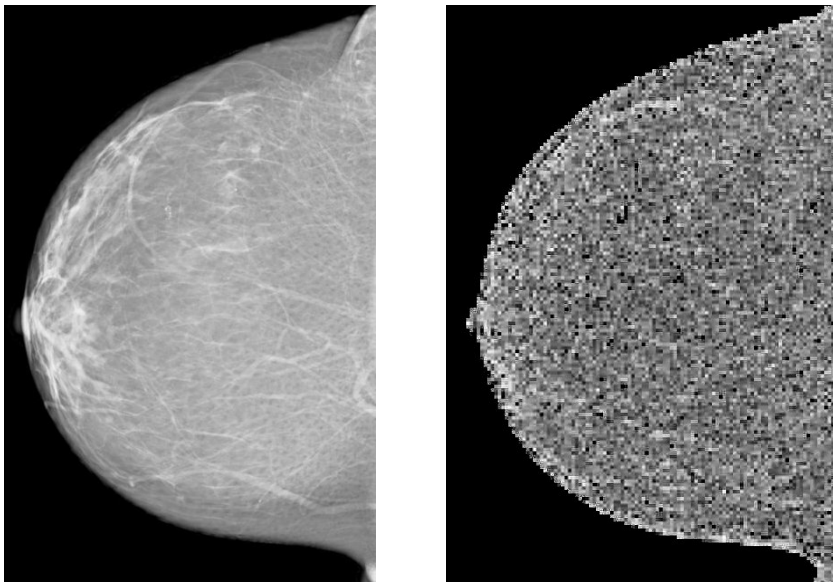

Fig. 2. The clinical mammogram of the patient from Fig. 1 (left) and the corresponding map of the entropy texture feature (right)

Fig. 3 shows the regression analysis results. A borderline statistical significance was observed for three texture features (features 9-11, p-values between 0.05 and 0.1); three additional features (features 17, 20, 24) had p-values between 0.1 and 0.15. It is likely that statistical significance was not achieved due to the limited sample size; thus, we are prevented from drawing a definitive conclusion about the correlation between texture and topology. The observed results, however, suggest a possible correlation between topological descriptors and several texture features. The bootstrap analysis of a hypothetically enlarged dataset with a sample size of 26 suggests that a statistically significant regression (at a significance level of 0.05) could be achieved between various texture features and topological descriptors. Fig. 3 shows the p-values from the bootstrap analysis.

The potential for inter-correlation between individual texture features was accounted for by applying PCA before performing the regression analysis, as PCA uses orthogonal transformations to convert the original data into a set of linearly uncorrelated variables. The bootstrap analysis performed in this paper to estimate the effect of sample size, assumed the noise in the enlarged data set to have a standard deviation equal to 50% of the standard deviation in individual sample data.

The results presented in this paper are based upon an initial analysis of 13 patients. We are currently analysing a larger set of clinical breast images; we expect to double the sample size in the near future. If the linear dependence between the texture and topology is confirmed (as suggested from our initial analysis and supported by bootstrapping), texture descriptors could be used as a proxy for topology, since the ductal network is not routinely visible in clinical images. Identifying texture features, or

combinations of texture features, which have the strongest correlation with topology could improve the understanding of texture-based risk biomarkers.

If, however, the increased sample size does not confirm the correlation between topology and texture, it could suggest that topology may carry risk-related information independent from texture descriptors. This could potentially lead to an improvement in the accuracy of breast cancer risk estimation techniques, assuming a clinically feasible method for the visualization and characterization of breast ducts (e.g., MRI or tomosynthesis) is available.

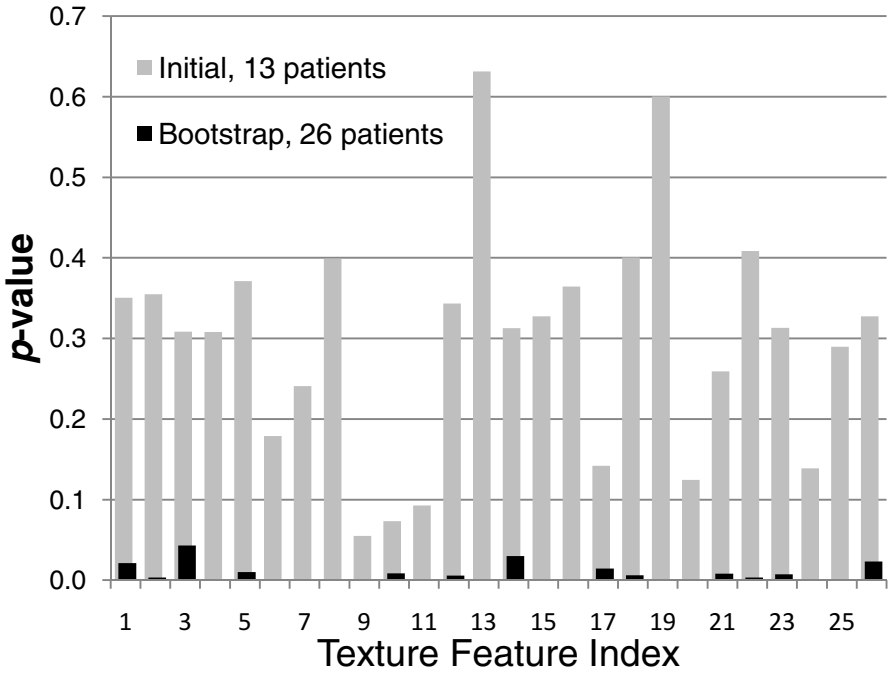

Fig. 3. *p*-value for the regression of individual texture features (averaged over all mammograms of the same patient) as a function of principal component analysis (PCA) components for the topological descriptors (tf-idf weights, averaged of all the traced ductal networks of the same patient). Shown are the results of the initial analysis of 13 patients, as well as the bootstrap results modelling a dataset of 26 cases.

It is worth noting the limitations of the current study. First, the ductal trees analysed in this paper were manually-traced from digitized galactograms. The manual tracing was performed by one person (a third-year medical student with experience in breast imaging). We believe that manual tracing did not compromise the analysis. In our previous study of ductal topology, we observed relatively low variations (a root-mean-square fractional error on the order of 2%) in estimated topological features due to manual tracing (2).

Additional potential limitations include the use of average texture descriptors, and the inter-correlation between individual descriptors of texture (or topology). In this paper, the regression analysis was performed using texture features averaged over the breast region in each mammographic image. These average values may suppress the differences in feature histograms calculated over mammographic images. In the future, we may repeat the analysis based upon other histogram moments, or using the full histogram as the texture descriptor.

4 Conclusion

We have performed a regression analysis between topological descriptors of the breast ductal network extracted from previously acquired, anonymized clinical galactograms, and texture descriptors estimated from corresponding clinical mammograms. Ductal networks were extracted from galactograms by manual tracing. The texture features were estimated using a fully automated image analysis pipeline. Initial analysis of clinical images from 13 women suggests correlation with borderline significance for a subset of texture descriptors. The identified subset of texture descriptors could hypothetically be used as proxy for ductal topological properties. Analysis of a larger number of clinical cases is ongoing.

Acknowledgments. This work was supported in part by the US National Science Foundation (III grant # 0916690 and CREST grant #HRD-0630388), the US National Institutes of Health (R01 grant #CA154444), the US Department of Defense Breast Cancer Research Program (HBCU Partnership Training Award #BC083639), and the US Department of Defense/Department of Army (45395-MA-ISP, #54412-CI-ISP, W911NF-11-2-0046), and the Delaware IDeA Network of Biomedical Research Excellence award. The content is solely the responsibility of the authors and does not necessarily represent the official views of the NIH, NSF and DoD.

References

[1] Bakic, P.R., Albert, M., Maidment, A.D.: Classification of galactograms with ramification matrices: Preliminary results. Academic Radiology 10(2), 198–204 (2003)

[2] Bakic, P.R., Albert, M., Brzakovic, D., Maidment, A.: Mammogram synthesis using a three-dimensional simulation. III. Modeling and evaluation of the breast ductal network. Medical Physics 30(7), 25–1914 (2003)

[3] Megalooikonomou, V., Barnathan, M., Kontos, D., Bakic, P.R., Maidment, A.D.A.: A Representation and Classification Scheme for Tree-Like Structures in Medical Images: Analyzing the Branching Pattern of Ductal Trees in X-ray Galactograms. IEEE Transactions on Medical Imaging 28(4), 93–487 (2009)

[4] Atwood, C.S., Hovey, R.C., Glover, J.P., Chepko, G., Ginsburg, E., Robison, W.G., et al.: Progesterone induces side-branching of the ductal epithelium in the mammary glands of peripubertal mice. Journal of Endocrinology 167(1), 39–52 (2000)

[5] Dinkel, H.P., Trusen, A., Gassel, A.M., Rominger, M., Lourens, S., Muller, T., et al.: Predictive value of galactographic patterns for benign and malignant neoplasms of the breast in patients with nipple discharge. British Journal of Radiology 73(871), 14–706 (2000)
[6] Cardenosa, G., Doudna, C., Eklund, G.: Ductography of the breast: technique and findings. America Journal of Roentgenology 162, 7–1081 (1994)
[7] Wolfe, J.N.: Breast patterns as an index of risk for developing breast cancer. American Journal of Roentgenology 126(6), 7–1130 (1976)
[8] Li, H., Giger, M.L., Huo, Z., Olopade, O.I., Lan, L., Weber, B.L., et al.: Computerized analysis of mammographic parenchymal patterns for assessing breast cancer risk: Effect of ROI size and location. Medical Physics 31(3), 55–549 (2004)
[9] Kontos, D., Bakic, P.R., Carton, A.-K., Troxel, A.B., Conant, E.F., Maidment, A.D.A.: Parenchymal Pattern Analysis in Digital Breast Tomosynthesis: Towards Developing Imaging Biomarkers of Breast Cancer Risk. Academic Radiology 16(3), 98–283 (2008)
[10] Bakic, P.R., Albert, M., Brzakovic, D., Maidment, A.D.A.: Mammogram synthesis using a 3D simulation. I. Breast tissue model and image acquisition simulation. Medical Physics 29(9), 9–2131 (2002)
[11] Pokrajac, D.D., Maidment, A.D.A., Bakic, P.R.: Optimized generation of high resolution breast anthropomorphic software phantoms. Medical Physics 39(4), 302–2290 (2012)
[12] Abbey, C.K., Bakic, P.R., Pokrajac, D.D., Maidment, A.D.A., Eckstein, M.P., Boone, J.: Non-Gaussian Statistical Properties of Virtual Breast Phantoms. In: Mello-Thoms, C.R., Kupinski, M.A. (eds.) SPIE Image Processing, Observer Performance, and Technology Assessment, vol. 9037. SPIE, San Diego (2014)
[13] Zheng, Y., Wang, Y., Keller, B.M., Conant, E.F., Gee, J.C., Kontos, D.: A fully-automated software pipeline for integrating breast density and parenchymal texture analysis for digital mammograms: Parameter optimization in a case-control breast cancer risk assessment study. In: Novak, C.L., Aylward, S. (eds.) SPIE Computer-Aided Diagnosis, vol. 8670. SPIE, Lake Buena Vista (2013)
[14] Devore, J.: Probability and Statistics for Engineering and the Sciences. Brooks/Cole, Belmont (2008)
[15] Efron, B.: The jackknife, the bootstrap and other resampling plans, Philadelphia, PA (1982)